JEM Journal of Experimental Medicine

ARTICLE

Viral MHCI inhibition evades tissue-resident memory T cell formation and responses

Elvin J. Lauron[1], Liping Yang[1], Ian B. Harvey[2], Dorothy K. Sojka[1], Graham D. Williams[3], Michael A. Paley[1], Michael D. Bern[1], Eugene Park[1], Francisco Victorino[1], Adrianus C.M. Boon[2,3], and Wayne M. Yokoyama[1,2]

Tissue-resident memory CD8⁺ T cells (T_{RM}s) confer rapid protection and immunity against viral infections. Many viruses have evolved mechanisms to inhibit MHCI presentation in order to evade CD8⁺ T cells, suggesting that these mechanisms may also apply to T_{RM}-mediated protection. However, the effects of viral MHCI inhibition on the function and generation of T_{RM}s is unclear. Herein, we demonstrate that viral MHCI inhibition reduces the abundance of CD4⁺ and CD8⁺ T_{RM}s, but its effects on the local microenvironment compensate to promote antigen-specific CD8⁺ T_{RM} formation. Unexpectedly, local cognate antigen enhances CD8⁺ T_{RM} development even in the context of viral MHCI inhibition and CD8⁺ T cell evasion, strongly suggesting a role for in situ cross-presentation in local antigen-driven T_{RM} differentiation. However, local cognate antigen is not required for CD8⁺ T_{RM} maintenance. We also show that viral MHCI inhibition efficiently evades CD8⁺ T_{RM} effector functions. These findings indicate that viral evasion of MHCI antigen presentation has consequences on the development and response of antiviral T_{RM}s.

Introduction

CD8⁺ T cells mediate potent immunity against viral infections and respond to foreign antigens presented by major histocompatibility complex class I (MHCI) molecules (Schmitz et al., 1999; Shoukry et al., 2003; Simon et al., 2006). The importance of MHCI antigen presentation is underscored by the fact that viruses have evolved strategies to block MHCI presentation. For instance, cowpox virus (CPXV) inhibits MHCI presentation by two distinct mechanisms. The CPXV203 protein retains MHCI molecules in the ER (Byun et al., 2007), whereas the CPXV012 protein prevents the transporter associated with antigen processing from loading antigen peptides onto MHCI molecules (Alzhanova et al., 2009; Byun et al., 2009). When combined, these mechanisms result in effective evasion of CD8⁺ T cell responses in vivo, and the absence of the CPXV012 and CPXV203 significantly attenuates CPXV in a CD8⁺ T cell–dependent manner (Byun et al., 2009; Gainey et al., 2012; Lauron et al., 2018). Moreover, the ability to inhibit MHCI presentation appears to be an evolutionarily conserved feature, though mechanistically distinct, among CMVs and other viruses (Hansen and Bouvier, 2009). Viral MHCI inhibition evades CD8⁺ T cell responses against murine CMV infection in the salivary glands of naive hosts and is critical in allowing for rhesus CMV superinfection of hosts harboring memory CD8⁺ T cells (Lu et al., 2006; Hansen et al., 2010). However, tissue-resident memory CD8⁺ T cells (T_{RM}s) are able to protect against local infection when murine CMV is directly introduced into the salivary glands, likely due to an early viral tropism for cells refractory to viral MHCI inhibition (Thom et al., 2015). Therefore, the effects of viral MHCI inhibition on CD8⁺ T_{RM} responses remain unclear.

CD8⁺ T_{RM}s typically form in nonlymphoid tissues following viral infection and are a noncirculating subset of memory T cells, whereas the effector memory T cell (T_{EM}) and central memory T cell (T_{CM}) subsets continuously recirculate (Carbone, 2015). Because CD8⁺ T_{RM}s primarily develop and remain at common sites of pathogen entry, they are considered a frontline defense against secondary or recurrent peripheral infections; both CD8⁺ and CD4⁺ T_{RM}s promote viral control and survival against lethal infection, mediate cross-strain protection, and even provide better protection than the circulating T_{EM} and T_{CM} counterparts (Gebhardt et al., 2009; Teijaro et al., 2011; Jiang et al., 2012; Mackay et al., 2012; Wu et al., 2014; Zens et al., 2016).

The factors driving T_{RM} development have implications for tissue-specific vaccine strategies. For example, the "prime and pull" strategy demonstrates that CD8⁺ T cells can be recruited to the skin or vagina in an antigen-independent manner and drive T_{RM} formation, resulting in long-term immunity against local challenge (Mackay et al., 2012; Shin and Iwasaki, 2012).

[1]Division of Rheumatology, Department of Medicine, Washington University School of Medicine, St. Louis, MO; [2]Department of Pathology and Immunology, Washington University School of Medicine, St. Louis, MO; [3]Department of Molecular Microbiology, Washington University School of Medicine, St. Louis, MO.

Correspondence to Wayne M. Yokoyama: yokoyama@wustl.edu.

Conversely, recruitment or inflammation alone does not generate T_{RM}s in the lungs unless local cognate antigen is present (Takamura et al., 2016; McMaster et al., 2018), indicating tissue-specific requirements for local cognate antigen during T_{RM} differentiation. Depots of persisting viral antigens in the lung may also affect the maintenance of memory T cells (Zammit et al., 2006; Lee et al., 2011). However, it is unknown whether persistent antigen presentation occurs in the skin or if MHCI complexes are important for the maintenance of endogenous skin $CD8^+$ T_{RM}s. In the context of viral infections, local cognate antigen recognition promotes the formation of $CD8^+$ T_{RM}s in the skin and is required for $CD8^+$ T_{RM} formation in the central nervous system, peripheral nervous system, and lungs (Wakim et al., 2010; Mackay et al., 2012; Khan et al., 2016; Muschaweckh et al., 2016; Pizzolla et al., 2017).

These findings on the potential role of local antigen during viral infection raise an interesting question: can viral MHCI inhibition affect local antigen recognition and reduce $CD8^+$ T_{RM} formation? To investigate this issue, we compared $CD8^+$ T_{RM} formation and protection following local infection with CPXV and a CPXV mutant lacking the capacity to inhibit MHCI presentation. Surprisingly, viral MHCI inhibition affected $CD4^+$ T_{RM} formation, but not the overall development $CD8^+$ T_{RM} formation, in the skin. We found that local secondary antigenic stimulation promoted $CD8^+$ T_{RM} formation, despite CPXV-mediated MHCI inhibition and $CD8^+$ T cell evasion. After T_{RM} differentiation, local cognate antigen presentation was dispensable for T_{RM} maintenance but was critical in infected cells to induce protective $CD8^+$ T_{RM} responses.

Results

Viral MHCI inhibition affects the formation of $CD4^+$ T_{RM}s but not $CD8^+$ T_{RM}s

CPXV-mediated MHCI inhibition could reduce local antigenic stimulation of virus-specific $CD8^+$ T cells by infected cells. Because local antigenic stimulation enhances $CD8^+$ T_{RM} formation during vaccinia virus (VACV) skin infection (Khan et al., 2016), we hypothesized that $CD8^+$ T_{RM} formation would be diminished in CPXV-infected skin. To test this, we infected mice by skin scarification (s.s.) with WT CPXV or Δ12Δ203 CPXV, which does not inhibit MHCI antigen presentation, and performed kinetic analyses of $CD8^+$ T cells that recognize the immunodominant H-$2K^b$–restricted epitope $B8_{19-26}$. Infection with both viruses resulted in robust expansion and recruitment of $B8_{19-26}$-specific $CD8^+$ T cells to the skin 1 wk after infection, which were reduced in numbers ∼12-fold by 3 wk after infection (Fig. 1 A). Nonetheless, $B8_{19-26}$-specific $CD8^+$ T cells were still detectable in the skin and the spleens of previously infected mice long after clearance of the infection (Fig. 1, A–D). CPXV skin infections are highly localized and are cleared within 1–2 wk after infection (Gainey et al., 2012). Mice infected with WT CPXV had a higher relative abundance of $B8_{19-26}$-specific $CD8^+$ T cells in the skin at 7 d postinfection (dpi) in comparison to Δ12Δ203-infected mice (Fig. 1, C and D), but there were no significant differences in absolute numbers in the skin for all assessed time points.

Analysis of $B8_{19-26}$-specific $CD8^+$ T cells during the memory phase showed that they were predominantly located in the previously infected skin flank relative to the uninfected contralateral flank (Fig. 1 B). These findings are consistent with previous reports (Gebhardt et al., 2009; Khan et al., 2016; Muschaweckh et al., 2016). We show that these cells expressed higher levels of the T_{RM} markers CD103 and CD69 than the $B8_{19-26}$-specific $CD8^+$ T cells in the spleen (Fig. 1, E and F), suggesting that CPXV s.s. infection generates authentic $CD8^+$ T_{RM}s. To verify tissue residency of $CD103^+CD69^+CD8^+$ cells, we performed parabiosis between $CD45.1^+$ naive mice and $CD45.2^+$ mice previously infected with CPXV, referred to as naive and memory mice, respectively (Fig. 1 G). Comparison of the $CD45.2^+CD45.1^-CD103^+CD69^+CD8^+$ T_{RM}s in the skin of naive and memory parabionts revealed the presence of these cells in only the memory parabionts, showing that they are unable to circulate and are indeed a resident population (Fig. 1, H and I). Furthermore, $CD45.2^+CD45.1^-B8_{19-26}$-tetramer$^+$ cells in the spleens equilibrated between memory and naive parabionts, but $CD45.2^+CD45.1^-B8_{19-26}$-tetramer$^+$ T_{RM}s in the skin were only present in memory parabionts (Fig. 1, J and K). Regarding $CD4^+$ T_{RM}, CPXV s.s. generated $CD103^+CD69^+CD4^+$ T cells in the skin in comparable numbers to $CD8^+$ T_{RM}, and parabiosis revealed that these cells were bona fide skin-resident $CD4^+$ T cells (Fig. 2, A–C). Interestingly, we found that viral MHCI inhibition significantly reduced the abundance of these $CD103^+CD69^+CD4^+$ T cells in the skin (Fig. 2, A and B). Taken together, these results reveal that viral MHCI inhibition does not affect the overall development of $CD8^+$ T_{RM}s but does impair the formation of $CD4^+$ T_{RM}s in the skin.

We reasoned that the effects of viral MHCI inhibition on local CPXV-specific $CD8^+$ T cells might have direct or indirect consequences on the development of $CD4^+$ T_{RM}s. To gain insight into how viral MHCI inhibition affects local antigen-specific $CD8^+$ T cells, we performed RNA sequencing (RNA-seq) on $B8_{19-26}$-specific $CD8^+$ T cells isolated from the skin and spleen of mice coinfected with WT CPXV and Δ12Δ203 on opposite flanks. At 7 dpi, $B8_{19-26}$-specific $CD8^+$ T cells isolated from WT CPXV and Δ12Δ203-infected skin exhibited similar expression profiles and shared many differentially expressed genes relative to splenic $B8_{19-26}$-specific $CD8^+$ T cells (Fig. S1, A and B). Gene set enrichment analysis (GSEA) of unique differentially expressed genes revealed significant enrichment of genes associated with activation of lymphocytes in Δ12Δ203-infected skin, while analysis of $B8_{19-26}$-specific $CD8^+$ T cells from WT CPXV–infected skin demonstrated expression of genes involved in the regulation of cytokine production (Fig. S1 C). Cytokines that were significantly up-regulated in WT CPXV–infected skin were also significantly up-regulated in Δ12Δ203-infected skin (Fig. S1 D). However, we found that IL-10 expression by $B8_{19-26}$-specific $CD8^+$ T cells was significantly higher in WT-infected skin in comparison to Δ12Δ203-infected skin, both at the transcript and protein levels (Fig. S1, E–G). The increased IL-10 production correlates with the reduced number of $CD4^+$ T_{RM} in WT CPXV–infected skin. IL-10 has been shown to reduce the number of circulating memory $CD4^+$ T cells following acute infection with lymphocytic choriomeningitis virus (Brooks et al., 2010). Therefore, these findings could explain why viral MHCI evasion affects $CD4^+$ T_{RM} formation.

$CD4^+$ T cell help is critical for the local development of lung $CD8^+$ T_{RM}s (Laidlaw et al., 2014) but dispensable for the forma-

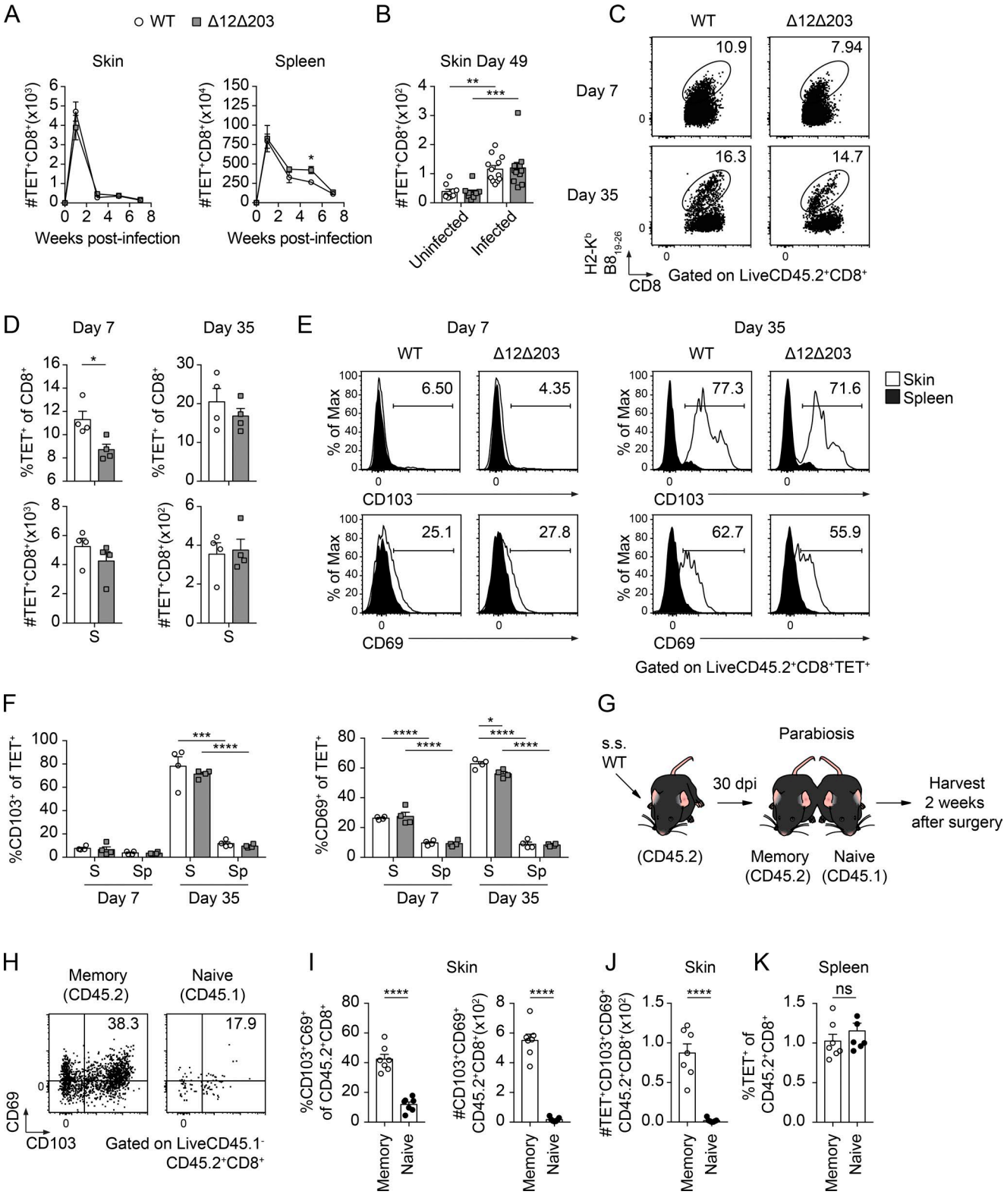

Figure 1. **Viral MHCI inhibition does not affect the overall development of CD8⁺ T_{RM}s. (A–F)** C57BL/6 mice were infected by s.s. with WT CPXV or Δ12Δ203. **(A)** The absolute number of $B8_{19–26}$-tetramer⁺ cells in the skin (S) and spleen (Sp) of infected mice over time (n = 4 mice per time point). **(B)** The absolute number of $B8_{19–26}$-tetramer⁺ cells in previously infected skin flank and the contralateral uninfected skin flank at 49 dpi. **(C)** Representative flow plots of $B8_{19–26}$-tetramer⁺ cells in the skin at the indicated time points. **(D)** Percentage (top) and absolute number (bottom) of $B8_{19–26}$-tetramer⁺ cells in the skin at 7 and 35 dpi. **(E)** Representative flow plots of CD103 and CD69 expression on $B8_{19–26}$-tetramer⁺ cells are shown for the indicated time points. **(F)** Percentage of CD103 (left) and CD69 (right) expression on $B8_{19–26}$-tetramer⁺ cells are shown for the indicated time points. **(G)** Schematic of the parabiosis experiment. **(H)** Representative flow plots of CD45.2⁺CD45.1⁻CD103⁺CD69⁺CD8⁺ T cells in the skin of parabiosed mice. **(I)** Percentage and absolute numbers of CD45.2⁺CD45.1⁻CD103⁺CD69⁺CD8⁺ T cells in the skin of parabiosed mice. **(J)** Absolute number of CD45.2⁺CD45.1⁻$B8_{19–26}$-tetramer⁺ T_{RM}s in the skin of parabiosed mice. **(K)** Percentage

tion of CD8$^+$ T_{RM}s in the female reproductive tract (Beura et al., 2018). To test the role of CD4$^+$ T cell help in the development of CD8$^+$ T_{RM} in the skin, we depleted CD4$^+$ T cells by injecting depleting antibodies 1 d before infection and then 2 and 5 dpi. This approach eliminates CD4$^+$ T cells during acute infection but allows for their recovery by 30 dpi. CD4$^+$ T cell help was not required for priming of CD8$^+$ T cells in the presence or absence of viral MHCI inhibition (Fig. 2, D and E). In accordance with our previous findings (Byun et al., 2009; Gainey et al., 2012), we found that mice infected with WT CPXV by s.s. succumbed to infection in the absence of CD4$^+$ T cell help (Fig. 2 F), despite the mounting an anti-CPXV CD8$^+$ T cell response (Fig. 2 E). These results underline the capacity of CPXV to efficiently evade CD8$^+$ T cells and suggest that CD4$^+$ T cell help is required to control localized CPXV infection. In contrast, all mice infected with Δ12Δ203 survived in the absence of CD4$^+$ T cell help (Fig. 2 F), which is also consistent with our previous findings that CD8$^+$ T cells alone are sufficient to control CPXV infection only in the absence of viral MHCI inhibition (Byun et al., 2009; Gainey et al., 2012). Given that Δ12Δ203 did not cause mortality, this provided a setting to assess the role of CD4$^+$ T cells in skin CD8$^+$ T_{RM} development. As expected, depleting CD4$^+$ T cells during the primary response reduced the overall number of CD4$^+$ T cells in the skin of mice previously infected with Δ12Δ203 but did not affect the overall development of CD4$^+$ T_{RM}s, since the percentage of CD103$^+$CD4$^+$ T cells in the skin was similar in isotype control–treated mice (Fig. 2, G and H). However, it is possible that these are not tissue-resident cells and instead represent a different subset of CD4$^+$ T cells. Surprisingly, the formation of CD8$^+$ T_{RM}s was augmented in the absence of CD4$^+$ T cell help (Fig. 2, G–I), indicating that CD4$^+$ T cell help is not required for the generation of skin CD8$^+$ T_{RM}s and may even hinder their development.

Local cognate antigen enhances CD8$^+$ T_{RM} formation, despite effective viral MHCI inhibition and CD8$^+$ T cell evasion

Since CD8$^+$ T_{RM} development occurred despite viral MHCI inhibition, we tested if CD8$^+$ T_{RM} formation is independent of local antigen. To this end, we performed coinfections on opposite flanks with CPXV viruses that express either a WT (WT and Δ12Δ203-CPXV) or a variant of the immunodominant $B8_{19-26}$ epitope (B8Y3AF5A and Δ12Δ203B8Y3AF5A) that is not presented on MHCI (Lauron et al., 2018; Fig. 3 A). During the acute phase of infection, $B8_{19-26}$-specific CD8$^+$ T cells had modestly higher frequencies of CD69 expression in the skin where $B8_{19-26}$ was expressed in comparison to the skin where the $B8_{19-26}$ epitope was absent, whereas CD103 expression was unaffected (Fig. S2, A and B). Nonetheless, a similar percentage and number of $B8_{19-26}$-specific CD8$^+$ T cells were recruited to both infected skin flanks in a local antigen-independent manner (Fig. 3 B). This was also the case when coinfections were performed with Δ12Δ203 and Δ12Δ203B8Y3AF5A. At 35 dpi, however, $B8_{19-26}$-specific T_{RM}s were significantly enriched in the skin where $B8_{19-26}$ was locally expressed as compared with infection where $B8_{19-26}$ was locally absent (Fig. 3 C), even in the presence of CPXV-mediated MHCI inhibition. Furthermore, the abundance of total CD8$^+$ T_{RM} was equal on both flanks of coinfected mice (Fig. 3 D), suggesting that T_{RM} formation was only affected for $B8_{19-26}$-specific CD8$^+$ T cells. Taken together, these data indicate that local antigen does promote CD8$^+$ T_{RM} formation during CPXV infection, regardless of viral MHCI inhibition.

Viral MHCI inhibition affects CD8$^+$ T cell effector function, but not recognition of local cognate antigen

To identify the cells that could display local cognate antigen, we assessed CPXV tropism in the skin of mice infected by CPXV s.s. There was significant recruitment of leukocytes in the skin at 6 dpi (Fig. 4 A). The majority of infected cells were MHCII/CD45 double positive and composed of mainly CD11b$^+$ dendritic cells (DCs) and monocyte-derived DCs (moDCs; Fig. 4, B and C). Moreover, CPXV$^+$ and MHCII$^+$ cells were found in close proximity to CD8$^+$ cells (Fig. 4 D), suggesting that CD8$^+$ T cells may engage infected CD11b$^+$ DCs or moDCs at the site of infection, though viral MHCI inhibition should prevent virus-specific T cell stimulation. Consistent with this notion, DC line DC2.4 cells infected with WT CPXV do not stimulate IFN-γ production by CPXV-specific CD8$^+$ T cells in vitro (Fig. 4 E). This effect is dependent on CPXV012 and CPXV203, as CPXV-specific CD8$^+$ T cells co-cultured with Δ12Δ203-infected DC2.4 cells produced significantly higher levels of IFN-γ and up-regulated expression of Nur77 (Fig. 4 E), a transcription factor that is specifically induced upon TCR engagement (Moran et al., 2011). However, our results suggest that CPXV-specific CD8$^+$ T cells can receive antigenic stimulation at the site of infection in vivo (Fig. 3 C).

We therefore tested if our in vitro findings extend to in vivo infection by coinfecting IFN-γ.Thy1.1 knockin (KI) reporter mice with WT CPXV and Δ12Δ203 on opposite flanks. Similar to our in vitro results, CPXV s.s. resulted in significantly lower frequencies of IFN-γ–producing CD8$^+$ T cells in WT CPXV–infected skin in comparison to Δ12Δ203-infected skin (Fig. 4 F). Conversely, the expression of Nur77 and the frequency of Nur77$^+$CD8$^+$ T cells were not significantly different (Fig. S2 C and Fig. 4 F). We also found similar results following coinfection of Nur77 GFP reporter mice (Fig. S2 D). In accordance with our findings that local cognate antigen promotes T_{RM} formation (Fig. 3 C), these findings suggest that CD8$^+$ T cells recruited to CPXV-infected skin receive local cognate antigen stimulation in the context of viral MHCI inhibition. However, it still remained unclear whether CPXV-specific CD8$^+$ T cells could recognize infected target cells in vivo, so we performed an in vivo cytotoxicity assay. After transfer of infected targets to day 7–infected mice, ∼72% of Δ12Δ203-infected targets were rapidly killed, whereas only ∼3% of WT-infected targets were killed (Fig. 3, G and H). These data suggest that, as a consequence of viral MHCI inhibition, WT CPXV–infected targets provide little to no antigenic stimulation and may only

of CD45.2$^+$CD45.1$^-$$B8_{19-26}$-tetramer$^+$ cells in the spleen of parabiosed mice. Data are representative of three independent experiments (A–F) or were pooled from two independent experiments (H–K). Symbols represent individual mice. Error bars represent means ± SEM. *, P < 0.05, **, P < 0.01, ***, P < 0.001, ****, P < 0.0001; ns, not significant; unpaired Student's *t* test (A–D and I–K) or one-way ANOVA followed by Tukey's post-test comparison (F).

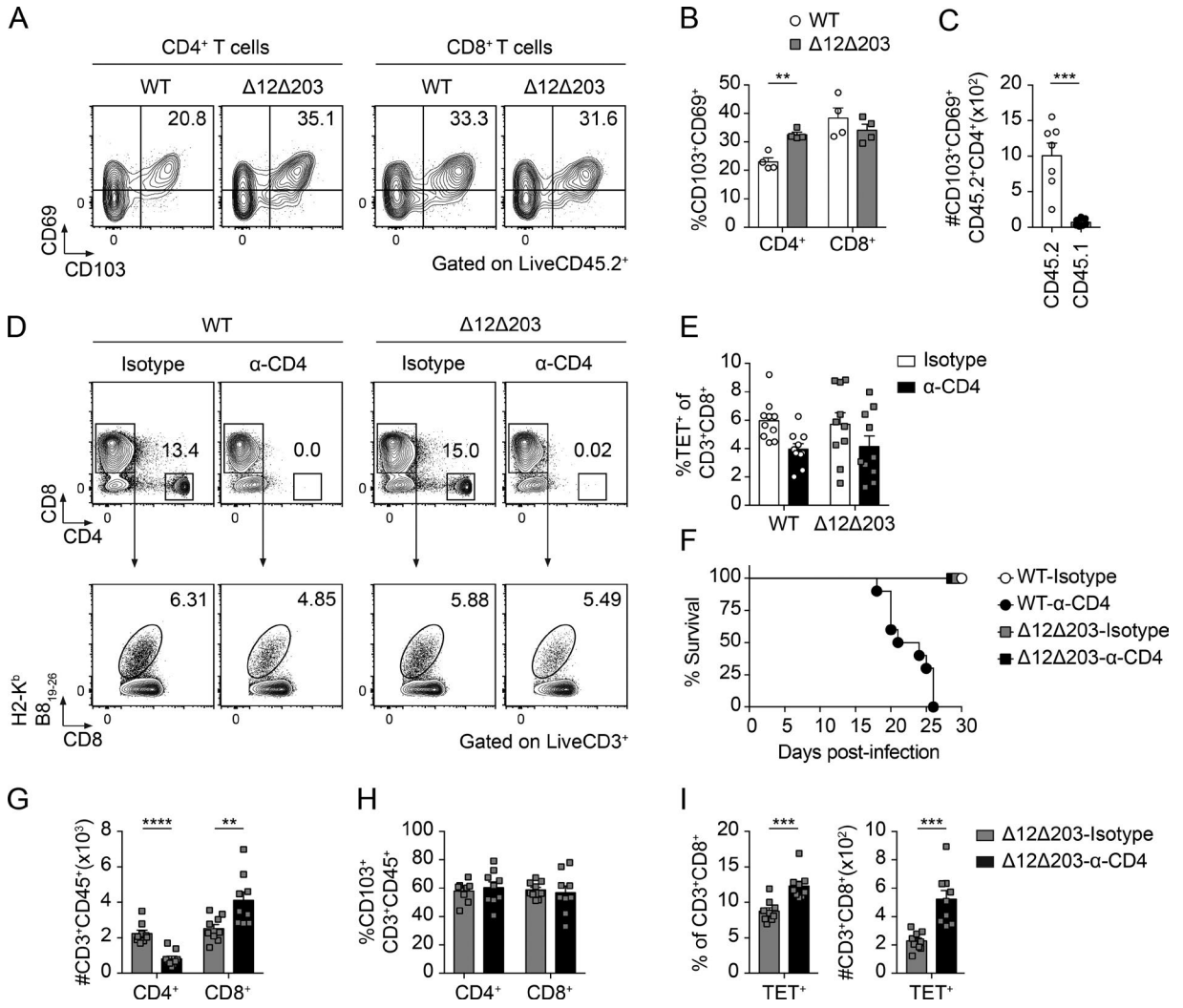

Figure 2. **Viral MHCI inhibition affects the formation of CD4⁺ T_{RM}s.** C57BL/6 mice were infected by s.s. with WT CPXV or Δ12Δ203. **(A)** Representative flow plots of CD103 and CD69 expression on CD4⁺ and CD8⁺ cells in the skin at 35 dpi. **(B)** Percentage of CD103⁺CD69⁺ T cells in the skin at 35 dpi. Data are representative of three independent experiments. **(C)** The absolute number of CD4⁺ T_{RM}s in the skin of parabiosed mice. Parabiosis was performed as outlined in Fig. 1 G. **(D–I)** Mice infected by s.s. with WT CPXV or Δ12Δ203 were treated with α-CD4 or isotype control antibodies on days −1, 2, and 5 after infection. **(D)** Representative flow plots of peripheral blood T cells and $B8_{19-26}$-tetramer⁺ cells at 7 dpi. **(E)** Percentage of $B8_{19-26}$-tetramer⁺ cells from peripheral blood at 7 dpi. **(F)** Percent survival (n = 10 mice per group). **(G)** Absolute number of CD4⁺ and CD8⁺ T cells in the skin at 30 dpi. **(H)** Percentage of CD103 expression on T cells at 30 dpi. **(I)** Percentage (left) and absolute numbers (right) of $B8_{19-26}$-tetramer⁺ cells in the skin at 30 dpi. Data are pooled from two independent experiments. Symbols represent individual mice. Error bars represent means ± SEM. **, P < 0.01, ***, P < 0.001, ****, P < 0.0001; ns, not significant; unpaired Student's t test (C–E and G–I) or one-way ANOVA followed by Tukey's post-test comparison (B).

contribute minimally to local antigen-driven T_{RM} differentiation. Strikingly, CD103⁺ DCs, which are essential for cross-priming of naive CPXV-specific CD8⁺ T cell precursors (Gainey et al., 2012; Lauron et al., 2018), remain largely uninfected following CPXV skin infection (Fig. 4 C) but were also found in close proximity to CD8⁺ cells at the site of infection (Fig. 4 D). These data strongly imply that CD8⁺ T cells in the skin are engaging cognate antigen on local cross-presenting cells.

Local antigen-driven CD8⁺ T_{RM} formation in the skin is limited by viral MHCI inhibition

Infection with WT CPXV is prolonged in comparison to Δ12Δ203 infection (Gainey et al., 2012), and it is therefore possible that during WT CPXV infection continuous recruitment of CD8⁺ T cells could compensate for decreased secondary antigenic stimulation on skin T_{RM} precursors. To test if continuous recruitment of CD8⁺ T cells to the skin augments CD8⁺ T_{RM} formation in the presence of viral MHCI inhibition, we used the sphingosine 1-phosphate receptor-1 (S1PR) agonist FTY720, which prevents lymphocyte egress from lymphoid and infected tissues. FTY720 treatment early during infection (1, 3, and 5 dpi) significantly reduced the presence of circulating CD8⁺ T cells in the blood and the recruitment of CD8⁺ T cells to infected skin, but not the priming of $B8_{19-26}$-specific CD8⁺ T cells in the inguinal lymph node (Fig. S3, A–C). FTY720 treatment also prolonged skin infection with both WT CPXV and Δ12Δ203, as indicated by lesion scab loss (Fig. S3, D and E), but Δ12Δ203-infected lesions still cleared slightly faster than WT CPXV–infected lesions.

We next performed coinfections of mice with WT CPXV and Δ12Δ203 on opposite flanks and then blocked CD8⁺ T cell recruit-

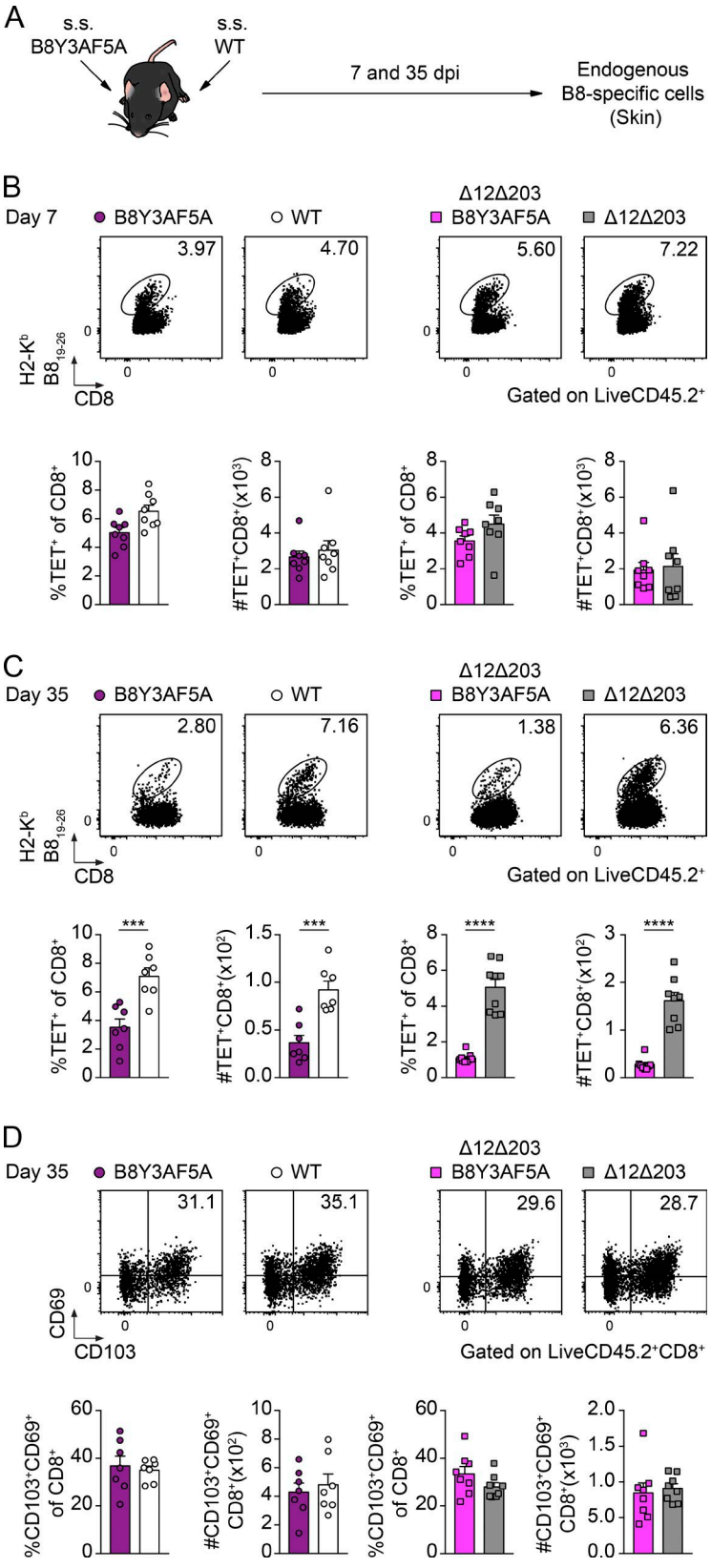

Figure 3. **Local cognate antigen enhances CD8⁺ T_{RM} formation, even in the context of viral MHCI inhibition and CD8⁺ T cell evasion. (A)** C57BL/6 mice were coinfected on opposite flanks by s.s. with $B8_{19–26}$-sufficient (WT or Δ12Δ203) and $B8_{19–26}$-deficient (B8Y3AF5A or Δ12Δ203B8Y3AF5A) CPXV. **(B)** Representative flow plots of $B8_{19–26}$-tetramer⁺ cells in the skin at 7 dpi are shown above the percentage and absolute number of $B8_{19–26}$-tetramer⁺ cells. **(C)** Representative flow plots of $B8_{19–26}$-tetramer⁺ cells in the skin at 35 dpi are shown above the percentage and absolute number of $B8_{19–26}$-tetramer⁺ cells. **(D)** Representative flow plots of CD103 and CD69 expression on CD8⁺ cells in the skin at 35 dpi are shown above the percentage and absolute number of CD103⁺CD69⁺CD8⁺ cells. Data are pooled from two independent experiments. Symbols represent individual mice. Error bars represent means ± SEM. ***, P < 0.001; ****, P < 0.0001; unpaired Student's *t* test.

ment to and egress from infected skin with FTY720 treatment starting at 7 dpi (Fig. S3 F). Starting FTY720 treatment at this later time point also prolonged the infection on both flanks of coinfected mice, yet lesion scab loss still occurred by 15 dpi (data not shown). While FTY720 significantly reduced the presence of CD4⁺ and CD8⁺ T cells in the blood of coinfected mice, the relative abundance of $B8_{19–26}$-specific CD8⁺ T cells at 9 dpi and CD8⁺ T_{RM}s at 40 dpi was not significantly different in WT CPXV– and Δ12Δ203-

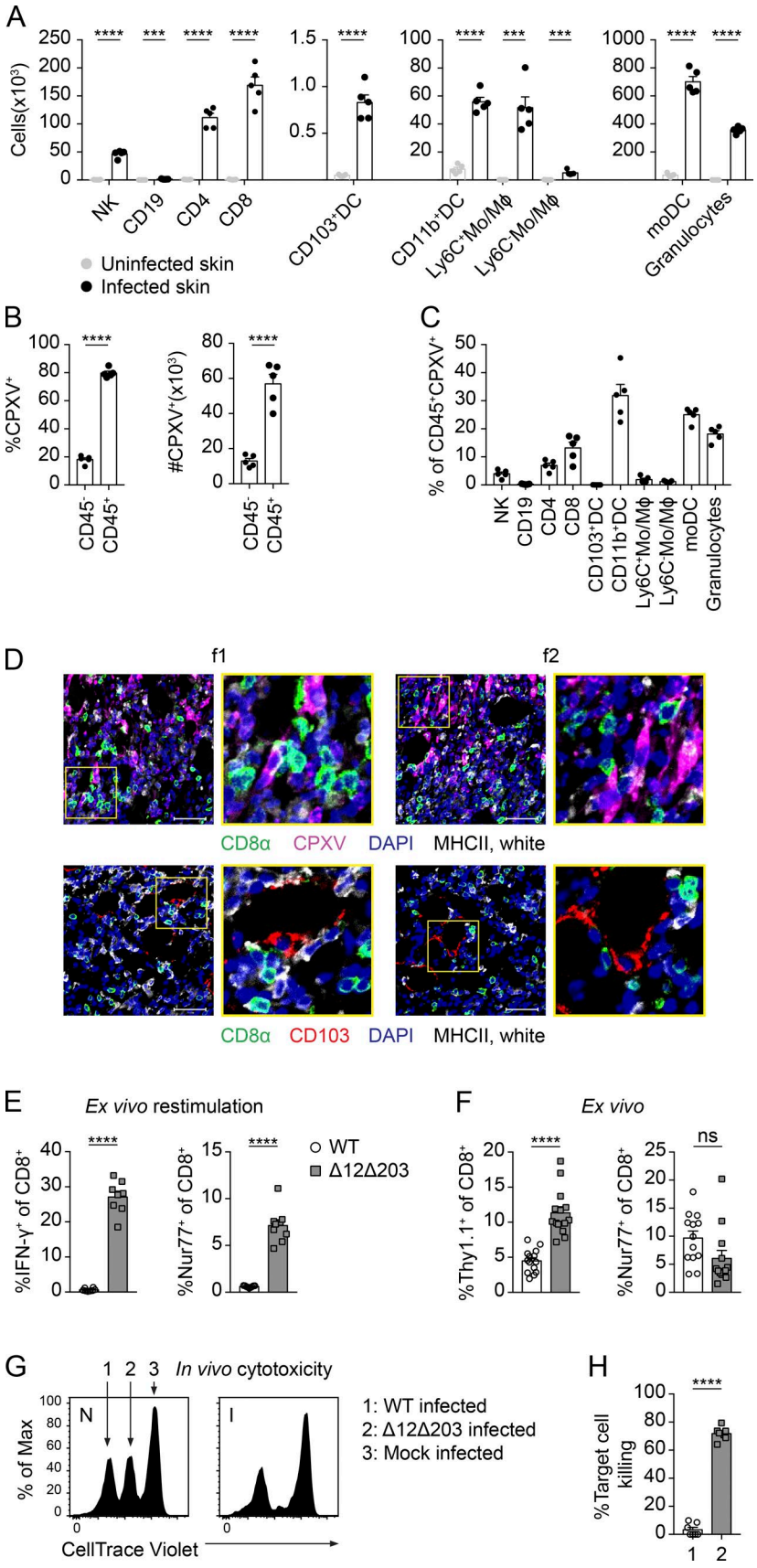

Figure 4. **Viral MHCI inhibition evades CD8⁺ T cell responses but does not affect TCR engagement with cognate antigen–MHCI complexes in vivo. (A–D)** C57BL/6 mice were infected by s.s. with WT CPXV and sacrificed on 6 dpi. **(A)** Absolute number of leukocytes recruited to WT CPXV–infected skin. Cells from the skin were gated on CD45⁺ and defined as follows: NK (CD3⁻CD19⁻NK1.1⁺), CD19 (CD3⁻CD19⁺), CD4 (CD19⁻CD3⁺CD4⁺), CD8 (CD19⁻CD3⁺CD8⁺), CD103⁺ DC (MHCII⁺CD11c⁺CD24⁺SIRPα⁻CD103⁺), CD11b⁺ DC (MHCII⁺CD24⁺CD64⁻CD11b⁺), Ly6C⁺ Mo/Mϕ (MHCII⁻CD64⁺CD11b⁺Ly6C⁺), Ly6C⁻ Mo/Mϕ (MHCII⁻CD64⁺CD11b⁺Ly6C⁻), moDCs (MHCII⁺CD11b⁺CD64⁺CD24⁺), and granulocytes (MHCII⁻CD24⁺CD11b⁺). Data are representative of two independent experiments. **(B)** Percentage and absolute number of CPXV⁺ cells, as determined by staining with α-VACV antibodies and flow cytometric analysis. Data are representative of two independent experiments. **(C)** Percentage of CPXV⁺ cells within the CD45⁺ populations. Data are representative of two independent experiments. **(D)** Immunofluorescence staining of CD8⁺, CD103⁺, CPXV⁺, and MHCII⁺ cells in the skin at 6 dpi. Bars, 50 µm. Data are representative of two independent experiments. **(E and F)** C57BL/6 mice or Thy1.1 KI IFN-γ reporter mice were coinfected with WT CPXV and Δ12Δ203. The spleens of infected C57BL/6 mice and skin of infected Thy1.1 KI IFN-γ reporter mice were harvested for ex vivo restimulation and direct ex vivo analyses, respectively, on 7 dpi. **(E)** Percentage of endogenous IFN-γ and Nur77 expression on CD8⁺ cells stimulated with WT CPXV– or Δ12Δ203-infected DC2.4 cells. Data are pooled from two independent experiments. **(F)** Percentage of IFN-γ (Thy1.1) and endogenous Nur77 expression on CD8⁺ cells from WT CPXV– or Δ12Δ203-infected skin. Data are pooled from three independent experiments. **(G and H)** DC2.4 cells were mock infected or infected with CPXV and used for in vivo cytotoxicity assays. Each group was differentially labeled and transferred i.v. to naive mice (N) or mice infected by s.s. for 7 d (I). **(G)** Representative flow plots of transferred cells harvested from the lungs of recipients 4 h after transfer. **(H)** Percent target killing from the in vivo cytotoxicity assay. Data are pooled from two independent experiments. Symbols represent individual mice. Error bars represent means ± SEM. ***, P < 0.001; ****, P < 0.0001; ns, not significant; unpaired Student's *t* test.

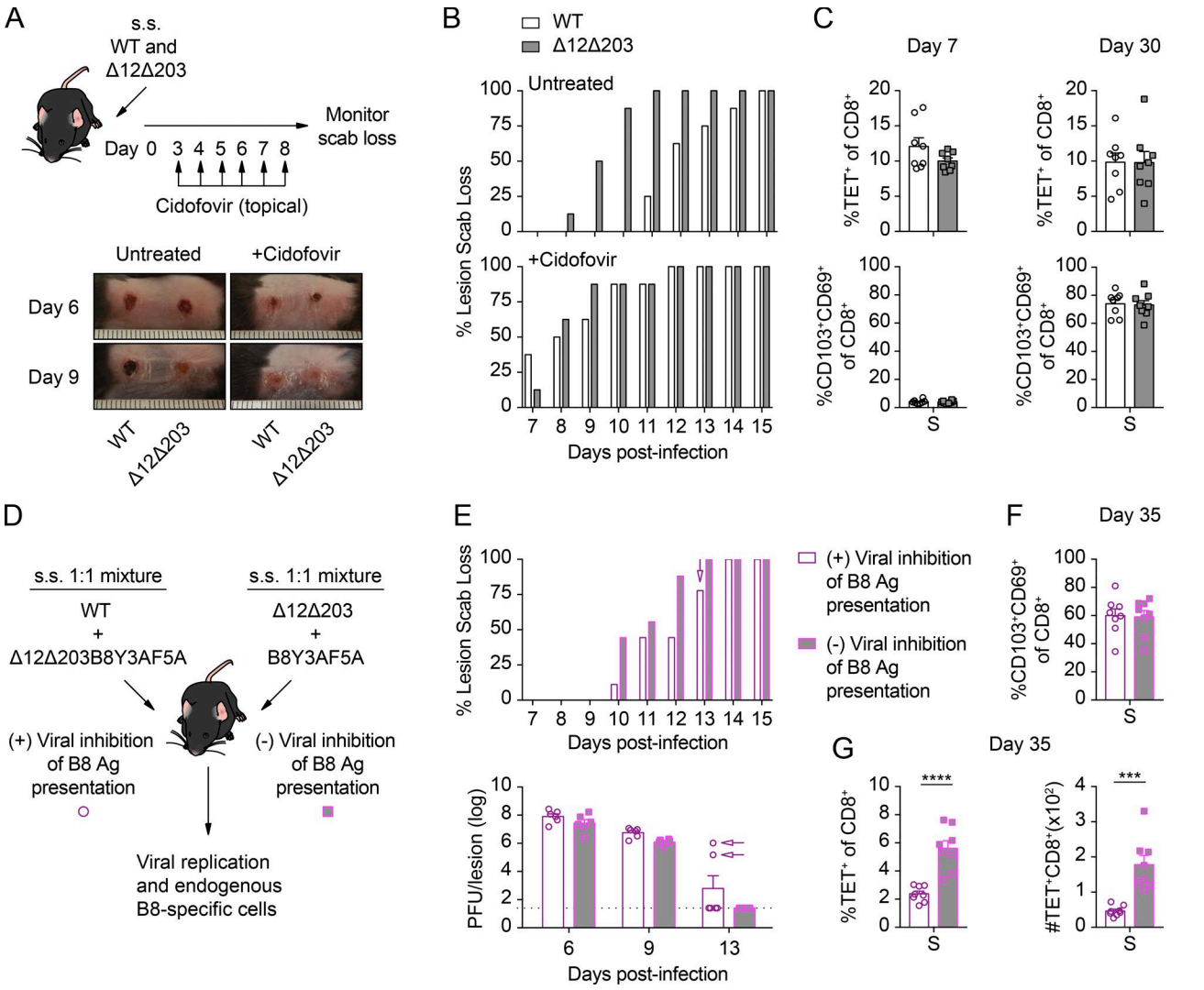

Figure 5. **Viral MHCI inhibition reduces local antigen-driven CD8⁺ T_{RM} formation in the skin. (A and B)** C57BL/6 mice were coinfected at adjacent sites with WT CPXV and Δ12Δ203, treated topically with a 1% cidofovir solution, and monitored for lesion scab loss (n = 8 mice per group). **(C)** C57BL/6 mice were infected by s.s. with WT CPXV or Δ12Δ203 and treated topically with cidofovir as outlined in A. Percentage of $B8_{19–26}$-tetramer⁺ cells (top) and CD103⁺CD69⁺CD8⁺ cells (bottom) in the skin at 7 dpi and 30 dpi. **(D)** C57BL/6 mice were coinfected on opposite flanks with two different mixtures of CPXV for F and G. **(E)** C57BL/6 mice were coinfected at adjacent sites with both mixtures. Lesion scab loss was monitored following coinfection of mice. Data are pooled from two independent experiments (n = 9 mice per group). Viral titers from skin lesions were determined by plaque assay. Arrows indicate mice that still had lesion scabs present at the indicated time point. **(F)** Percentage of CD103⁺CD69⁺CD8⁺ cells in the skin (S) at 35 dpi. **(G)** Percentage (left) and absolute number (right) of $B8_{19–26}$-tetramer⁺ cells in the skin at 35 dpi. Data are pooled from two independent experiments. Symbols represent individual mice. Error bars represent means ± SEM. ***, P < 0.001; ****, P < 0.0001; unpaired Student's t test.

infected skin, with or without FTY720 treatment (Fig. S3, G and H). These results indicate that CD8⁺ T_{RM}s develop without continuous recruitment of CD8⁺ T cells, which is consistent with the findings that recruitment or inflammation alone is sufficient to induce T_{RM} formation (Mackay et al., 2012; Shin and Iwasaki, 2012). However, differences in viral replication between WT CPXV and Δ12Δ203 may also influence T_{RM} development, making it difficult to assess the effects of viral MHCI inhibition on T_{RM} formation.

We therefore sought to uncouple the potential effects of prolonged viral replication and the effects of viral MHCI inhibition. To do so, we treated infected mice with the antiviral compound cidofovir. Topical treatment with cidofovir resulted in a faster rate of viral clearance in comparison to untreated control mice (Fig. 5, A and B). Moreover, WT CPXV– and Δ12Δ203-infected skin lesions were cleared at a similar rate with cidofovir treatment, whereas WT CPXV–infected skin lesions were cleared at a slower rate than Δ12Δ203-infected skin lesions in untreated control mice. Interestingly, cidofovir-treated mice infected with WT CPXV or Δ12Δ203 showed no differences in the abundance of $B8_{19–26}$-specific T_{RM}s, despite simultaneous viral clearance and equal acute recruitment of $B8_{19–26}$-specific CD8⁺ T cells in infected skin (Fig. 5 C).

We postulated that the effects of viral MHCI inhibition on the local microenvironment might also be a confounding variable. We therefore devised a coinfection approach in which the environment and viral replication could be better controlled in a setting where B8 antigen presentation is or is not inhibited by CPXV012 and CPXV203 (Fig. 5 D). For inhibited B8 antigen presentation, we infected one flank with a 1:1 mixture of WT

CPXV and Δ12Δ203B8Y3AF5A. In this mix, WT CPXV provides a setting with inhibited B8 antigen presentation, while Δ12Δ203B8Y3AF5A serves to control for the local infectious environment and the total amount of virus per infection site but does not contribute to B8 antigen load. For uninhibited B8 antigen presentation, we infected the opposite flank with a 1:1 mixture of Δ12Δ203 and B8Y3AF5A. Infection with Δ12Δ203 provides a source of uninhibited B8 Ag presentation, because it lacks the CPXV MHCI inhibitors. The B8Y3AF5A virus contains both MHCI inhibitors CPXV012 and CPXV203. It also serves as a control for the local infectious environment and has comparable viral clearance to WT CPXV, even though it does not contribute to B8 antigen load. Therefore, the effects of viral MHCI inhibition on the local microenvironment and the duration of infection for each mixture should be comparable. As expected, each mixture resulted in comparable total levels of viral replication and clearance, as determined by plaque assays and lesion scab loss (Fig. 5 E). At 35 dpi, the abundance of CD8$^+$ T_{RM}s was comparable under both conditions (Fig. 5 F). Remarkably, the abundance of $B8_{19-26}$-specific CD8$^+$ T_{RM}s was significantly reduced when B8 Ag presentation was inhibited by CPXV012 and CPXV203 (Fig. 5 G), indicating that viral MHCI inhibition does indeed affect local antigen-driven T_{RM} formation.

Viral MHCI inhibition reduces the amount of antigen-specific lung CD8$^+$ T_{RM}s

We next assessed the effects of CPXV-mediated MHCI inhibition on lung CD8$^+$ T_{RM}s, since the developmental requirements can differ substantially between certain tissue microenvironments (Pizzolla et al., 2017). To distinguish circulating memory CD8$^+$ T cells from T_{RM}s, we performed in vivo intravascular (IV) staining (Anderson et al., 2012). This method exclusively labels circulating and IV lymphocytes (IV$^+$ cells), but not tissue-associated lymphocytes (IV$^-$). Within the lung tissue, the overall proportions of IV$^-$CD8$^+$ T cells were equal in mice i.n. infected with WT CPXV or Δ12Δ203 at 12 and 30 dpi, suggesting that viral MHCI inhibition also does not affect the overall development of lung CD8$^+$ T_{RM}s (Fig. 6, A and B). In contrast, higher proportions of IV$^-$ $B8_{19-26}$-specific T_{RM}s were found in the lungs following Δ12Δ203 infection compared with WT CPXV infection (Fig. 6 C). This difference was also reflected in the spleen and blood at 30 dpi, despite equal proportions of $B8_{19-26}$-specific CD8$^+$ T cells in the spleen and blood at 12 dpi (Fig. 6, D and E). Viral MHCI inhibition also significantly reduced the expression of CD103 on IV$^-$ $B8_{19-26}$-specific CD8$^+$ T cells at 12 dpi, but not CD69 expression (Fig. 6, F and G). The reduced expression of CD103 did not appear to affect CD8$^+$ T_{RM} development, since IV$^-$ $B8_{19-26}$-specific CD8$^+$ T cells in the lungs of WT CPXV– and Δ12Δ203-infected mice expressed comparable levels of CD69 and CD103 by 30 dpi (Fig. 6, F and G). These data indicate that viral MHCI inhibition also reduces the formation of antigen-specific CD8$^+$ T_{RM}s in the lungs.

CD8$^+$ T_{RM}s in the skin persist in the absence of cognate antigen stimulation

Having established the importance of local cognate antigen in CD8$^+$ T_{RM} formation against CPXV, we questioned whether local cognate antigen plays a role after CD8$^+$ T_{RM} populations are established. To address this, we generated *B2m*$^{fl/fl}$RS26-Cre-ER^{T2} mice in which tamoxifen treatment ablates MHCI expression. *B2m*$^{fl/fl}$RS26-Cre-ER^{T2} mice infected by s.s. were treated with tamoxifen at 49 dpi, and CD8$^+$ T_{RM}s were analyzed in the skin ∼1 mo after treatment (Fig. 7 A). Tamoxifen treatment eliminated the expression of MHCI on CD45$^+$ cells from the skin and spleen of *B2m*$^{fl/fl}$RS26-Cre-ER^{T2} mice (Fig. 7 B), but not from tamoxifen-treated *B2m*$^{fl/fl}$ littermate controls. We detected $B8_{19-26}$-specific T_{RM}s at comparable levels in the skin of tamoxifen-treated *B2m*$^{fl/fl}$RS26-Cre-ER^{T2} and *B2m*$^{fl/fl}$ mice (Fig. 7 C), indicating that persistent antigen presentation is not required for CD8$^+$ T_{RM} maintenance. This was also observed for total CD8$^+$ T_{RM}s in the skin (Fig. 7 D). Furthermore, we assessed TCR engagement on CD8$^+$ T_{RM}s using the Nur77 GFP reporter mice and found that CD8$^+$ T_{RM}s are Nur77 negative (Fig. 7 E). Therefore, CD8$^+$ T_{RM}s do not receive cognate antigen stimulation in the skin and are maintained in an antigen-independent manner.

Viral MHCI inhibition evades local CD8$^+$ T_{RM} responses

Since viral MHCI inhibition evades CD8$^+$ T cell responses during primary CPXV infection, we next investigated the effects of viral MHCI inhibition on CD8$^+$ T_{RM} effector function in the absence of other anti-CPXV immune responses. To do so, we generated a recombinant influenza virus that expresses the CPXV $B8_{19-26}$ epitope (Flu-B8) and infected mice by the i.n. route. This resulted in the formation of $B8_{19-26}$-specific T_{RM}s in the lungs of infected mice at 30 dpi (Fig. S4). We next challenged the mice with CPXV at 30 dpi (Fig. 8 A). To prevent circulating memory CD8$^+$ T cells from contributing to viral control upon CPXV challenge, we treated Flu-B8–infected mice with FTY720 throughout the course of the CPXV challenge. Viral titers in the lungs of mice challenged with Δ12Δ203 were significantly lower than in mice challenged with WT CPXV (Fig. 8 B), demonstrating that viral MHCI inhibition abrogates protective CD8$^+$ T_{RM} responses in the lungs. Furthermore, CD8$^+$ T_{RM}–mediated protection was antigen dependent, since challenge with B8-deficient viruses resulted in titers comparable to challenge with WT CPXV.

To test if these findings also hold true during CPXV skin infection, we used μMT mice in order to avoid humoral responses against CPXV challenge, as these mice lack mature B cells. μMT mice previously infected by s.s. with Δ12Δ203 harbored few $B8_{19-26}$-specific T_{RM}s in the skin (Fig. S5, A and B), which is consistent with the findings that infection of μMT mice generates significantly lower numbers of memory CD8$^+$ T cells in comparison to infection of WT C57BL/6 mice (Asano and Ahmed, 1996; Shen et al., 2003). These findings are unlikely due to differences in viral replication or dissemination, since Δ12Δ203 replicates and is cleared in the μMT mice at comparable rates to C57BL/6 mice (Fig. S5, C and D). We next tested whether depleting CD4$^+$ T cells during acute infection of μMT mice would increase CD8$^+$ T_{RM} formation. Similar to what we observed in WT C57BL/6 mice (Fig. 2, G–I), depleting CD4$^+$ T cells significantly increased CD8$^+$ T_{RM} formation in the skin of μMT mice infected by s.s., but not i.n., infection (Fig. S5, A and B). In contrast, depleting CD4$^+$ T cells did not significantly increase the number of $B8_{19-26}$-specific CD8$^+$ T cells in the spleen of μMT mice previously infected by s.s.

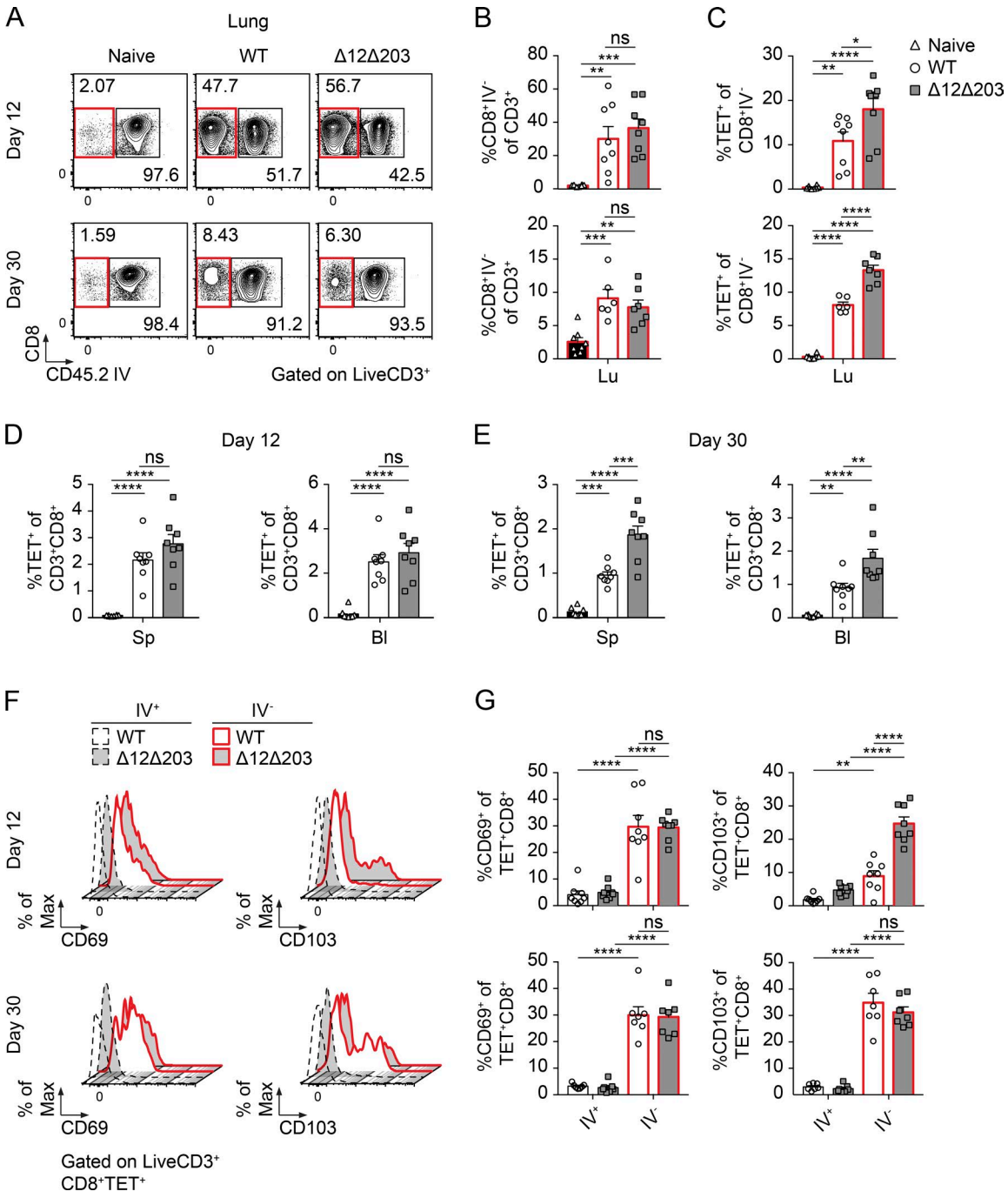

Figure 6. **Viral MHCI inhibition reduces the abundance of lung CD8⁺ T_{RM}.** C57BL/6 mice were infected i.n. with WT CPXV or Δ12Δ203. IV staining with an anti-CD45 antibody was performed before euthanizing mice at 12 and 30 dpi. **(A)** Representative flow plots of CD45 expression on CD8⁺ cells in the lungs (Lu). Data are representative of two independent experiments. **(B)** Percentage of IV⁻CD8⁺ cells in the lungs at 12 (top) and 30 (bottom) dpi. **(C)** Percentage of IV⁻CD8⁺$B8_{19–26}$-tetramer⁺ cells in the lungs at 12 (top) and 30 (bottom) dpi. **(D and E)** Percentage of CD8⁺$B8_{19–26}$-tetramer⁺ cells in the spleen (Sp) and blood (Bl) are shown at 12 and 30 dpi. **(F)** Representative flow plots of CD69 or CD103 expression on IV⁺/IV⁻ $B8_{19–26}$-tetramer⁺ cells at 12 and 30 dpi. **(G)** Percentage of CD69 and CD103 expression on IV⁺/IV⁻ $B8_{19–26}$-tetramer⁺ cells at 12 (top) and 30 (bottom) dpi. Data are pooled from two independent experiments. Symbols represent individual mice. Error bars represent means ± SEM. *, P < 0.05; **, P < 0.01; ***, P < 0.001; ****, P < 0.0001; ns, not significant; one-way ANOVA followed by Tukey's post-test comparison.

Based on these findings, we induced CD8⁺ T_{RM} formation in CD4⁺ T cell–depleted μMT mice by s.s. with Δ12Δ203 and subsequently challenged the skin with WT CPXV and Δ12Δ203 at 30 dpi (Fig. 8 C). Viral titers in the skin of naive mice were not significantly different in WT CPXV– and Δ12Δ203-infected lesions 4 d after challenge (Fig. 8 D). Similarly, viral titers were not significantly different in previously infected μMT mice lacking skin CD8⁺ T_{RM}s (i.n. infected). Conversely, μMT mice harboring skin CD8⁺ T_{RM}s (s.s. infected) presented viral titers that were significantly reduced by several logs in the Δ12Δ203 lesions (Fig. 8 D),

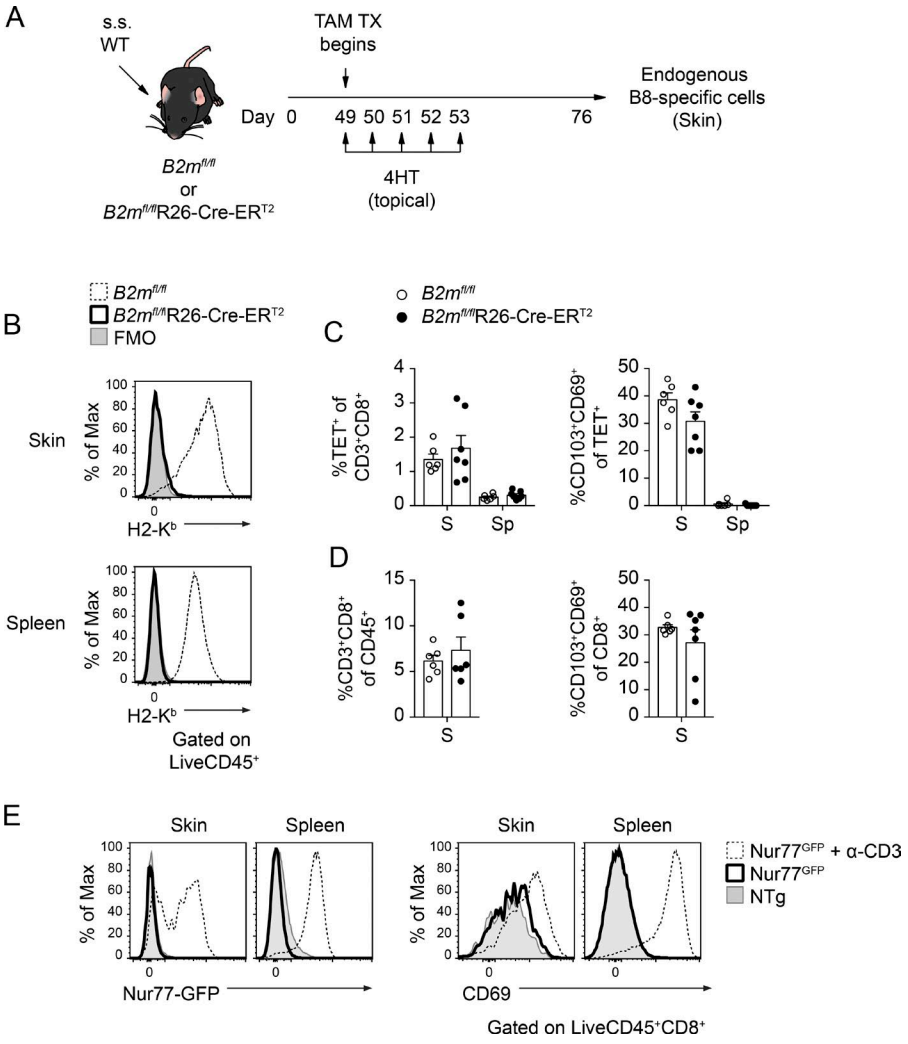

Figure 7. **CD8⁺ T_{RM}s are maintained in the absence of cognate antigen stimulation.** *B2m*$^{fl/fl}$RS26-Cre-ER^{T2} mice and *B2m*$^{fl/fl}$ littermate controls were infected by s.s. with WT CPXV. On 49 dpi, mice were started on a tamoxifen chow diet (TAM TX) and treated topically with 4HT daily for 5 d. Additionally, mice were treated with α-NK1.1 (100 µg/mouse) once weekly starting on 49 dpi to deplete NK cells. **(A–D)** Mice were euthanized at 76 dpi and CD8⁺ T cells were analyzed in the skin (S) and spleen (Sp). **(B)** Representative flow plots of H-2K^b expression on CD45⁺ cells from the skin and spleen on 76 dpi. **(C)** Percentage of B8$_{19–26}$-tetramer⁺ and CD103⁺CD69⁺ cells in the skin and spleen at 76 dpi. **(D)** Percentage of total CD8⁺ and CD103⁺CD69⁺ cells in the skin at 76 dpi. Data are pooled from two independent experiments. Symbols represent individual mice. Error bars represent means ± SEM. **(E)** Nur77^{GFP} reporter mice and nontransgenic (NTg) littermate controls were infected by s.s. with WT CPXV and euthanized at 30 dpi. CD8⁺ T cells were analyzed in the skin and spleen. As a positive control, B8 peptide was administered intradermally and an α-CD3 antibody was administered i.v. into Nur77^{GFP} mice previously infected for 30 d. Representative flow plots of Nur77 (GFP) and CD69 expression on skin and splenic CD8⁺ T cells are shown. Data are representative of three independent experiments; total *n* = 3 positive control mice, total *n* = 5 Nur77^{GFP} mice, and total *n* = 6 Ntg mice. Statistical significance was assessed using an unpaired Student's *t* test (D) or one-way ANOVA followed by Tukey's post-test comparison (C).

whereas WT CPXV titers were not significantly reduced in comparison to naive and i.n.-infected mice. The differences were also apparent by lesion formation (Fig. 8 D). These data demonstrate that CPXV effectively evades CD8⁺ T_{RM} responses, but CD8⁺ T_{RM}s can provide protection against CPXV in the absence of viral MHCI inhibition. Intriguingly, similar results were obtained in µMT mice that harbored fewer skin CD8⁺ T_{RM}s (isotype-treated controls), indicating that CD4⁺ T cell help is not required for the generation of functional skin CD8⁺ T_{RM}s (Fig. 8 E).

Discussion

In this study, we assessed the effects of viral MHCI inhibition on the generation and function of T_{RM}s using CPXV and the Δ12Δ203 mutant. Consistent with what was previously reported for VACV skin infection (Khan et al., 2016; Muschaweckh et al., 2016), local antigenic stimulation promoted CD8⁺ T_{RM} formation in CPXV-infected skin, indicating that the viral MHCI inhibitors CPXV012 and CPXV203 do not completely obstruct local antigenic stimulation of CD8⁺ T cells or subsequent CD8⁺ T_{RM} development. We note that the duration of local antigen exposure may be shorter throughout Δ12Δ203 infection than WT CPXV infection as a consequence of unimpeded clearance by CPXV-specific CD8⁺ T cells. Despite the potentially reduced window for antigen stimulation, Δ12Δ203 infection in both the skin and the lung significantly enhanced local antigen-driven T_{RM} formation compared with infection with WT CPXV, suggesting that early encounters with local antigen have greater effects on T_{RM} differentiation than the length or persistence of antigen presentation.

Our results also suggest that local antigenic stimulation of CD8⁺ T cells may promote CD8⁺ T_{RM} development without eliciting T cell–mediated cytotoxicity, raising the possibility that T_{RM} precursors receive local antigenic stimulation from cross-presenting cells in situ (Boissonnas et al., 2013; Broz et al., 2014). This possibility would explain why local antigen stimulation enhances T_{RM} formation that is not significantly affected by the presence of viral MHCI inhibition. Since cross-presentation by BATF3⁺ DCs imprints T_{RM} precursors in the lymph nodes (Iborra et al., 2016) and is required for CPXV-specific T cell priming (Gainey et al., 2012; Lauron et al., 2018), these cells are candidates for involvement in local cross-presentation; further investigation will be needed to determine their relative contribution to in situ cross-presentation during T_{RM} development. Intriguingly, our results also raise the possibility that local cross-presentation may be involved in activating skin CD8⁺ T_{RM} cytokine production.

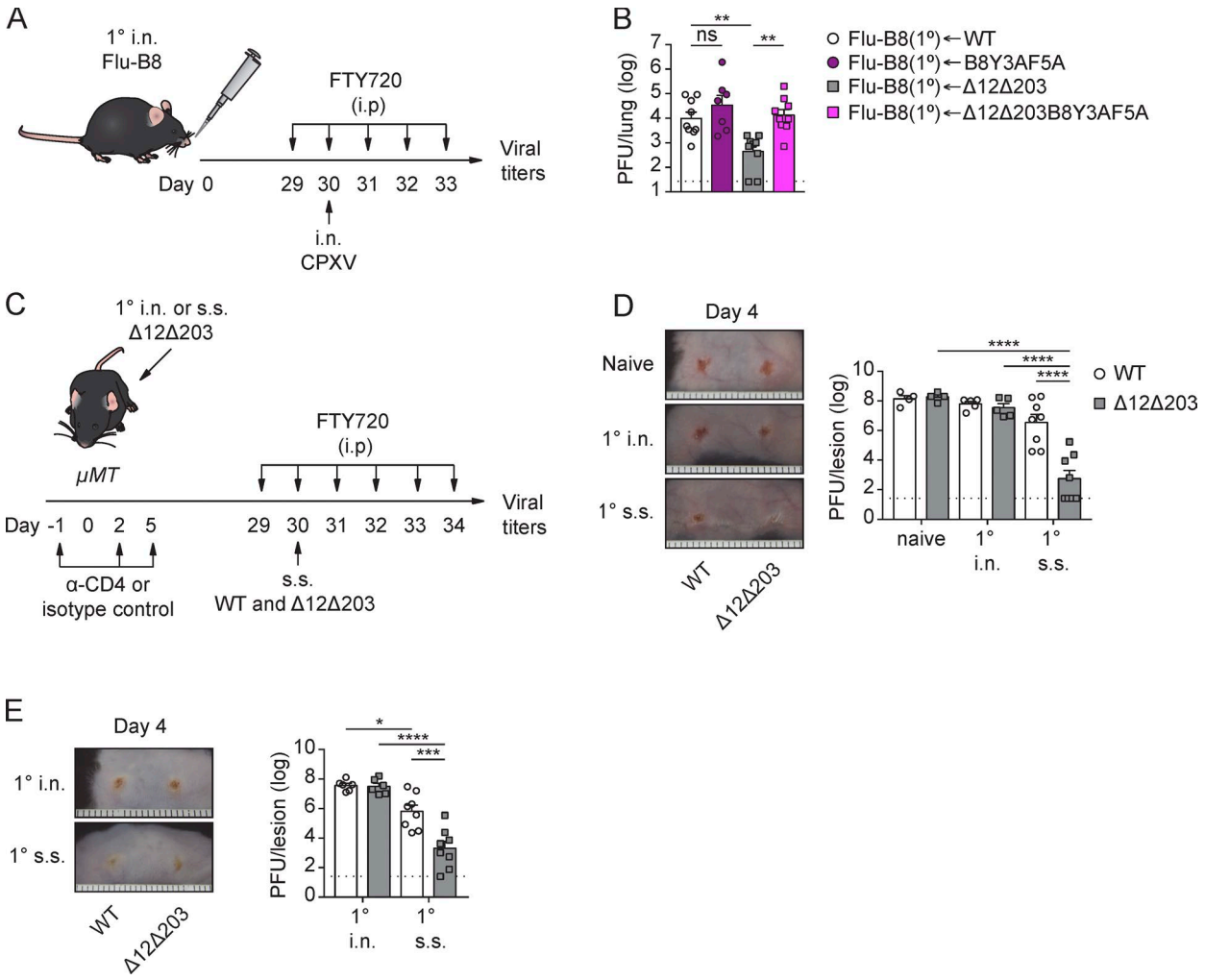

Figure 8. **Viral MHCI inhibition evades protective CD8⁺ T_{RM} responses. (A)** Schematic of the heterologous prime/challenge experiment. **(B)** Viral titers in the lungs of Flu-B8–immunized mice challenged with CPXV. Data are pooled from two independent experiments. **(C)** Schematic of μMT mice skin challenge experiment. **(D)** Image of infected flanks and viral titers from skin lesions 4 d after s.s. challenge of α-CD4–treated naive control and CPXV-immunized μMT mice. **(E)** Viral titers from skin lesions 4 d after s.s. challenge of isotype control–treated CPXV-immunized μMT mice. Data are pooled from two (B) or three (D and E) independent experiments. Symbols represent individual mice. Error bars represent means ± SEM. *, P < 0.05; **, P < 0.01; ***, P < 0.001; ****, P < 0.0001; ns, not significant; one-way ANOVA followed by Tukey's post-test comparison.

Local antigen presentation by APCs is critical for the activation of CD8⁺ T_{RM}s in the female genital tract and central nervous system (Wakim et al., 2010; Shin et al., 2016), but direct contact with infected target cells is not necessarily required for CD8⁺ T_{RM}–mediated protection. For instance, in situ peptide stimulation of CD8⁺ T_{RM}s is sufficient to induce a tissue-wide antiviral state and protects against antigenically distinct viruses (Ariotti et al., 2014; Schenkel et al., 2014). Therefore, CD8⁺ T_{RM} activation and protection can ensue independently of direct cell–cell contact with infected target cells. We found that CD8⁺ T_{RM} protection during viral infection is abrogated by viral MHCI inhibition, indicating that TCR/peptide-MHCI (pMHCI) stimulation via engagement of infected target cells is needed for optimal CD8⁺ T_{RM} functions. We also found that CD4⁺ T cell help was not required for the generation of functional skin CD8⁺ T_{RM}s and that the absence of CD4⁺ T cell help increased skin CD8⁺ T_{RM} formation. As T_{RM}s have been shown to compete within epidermal niches (Zaid et al., 2014), it is possible that the absence of CD4⁺ T cells during acute infection reduces competition for local survival signals and space, lessening the constraints on the number of CD8⁺ T_{RM}s.

Additionally, we show CD8⁺ T_{RM} development in the lungs of CPXV-infected mice remained largely unaffected by viral MHCI inhibition, but viral MHCI inhibition reduced the abundance of antigen-specific lung T_{RM}s. The induction of CPXV-specific CD8⁺ T cell responses is not affected by viral MHCI inhibition during primary CPXV infection (Gainey et al., 2012; Lauron et al., 2018), but the breadth and the levels of viral epitopes presented in this context can differ from those presented in the absence of viral MHCI inhibition (Basta et al., 2002; Shen et al., 2002). As a consequence, increased antigen presentation and antigen abundance during respiratory infection with Δ12Δ203 potentially promotes CD8⁺ T cell cross-competition for pMHCI complexes, which can affect the T_{RM} repertoire (Muschaweckh et al., 2016; Pizzolla et al., 2017). These findings were not found following CPXV skin infection, suggesting that differences in the microenvironment also play a role in the development of antigen-specific T_{RM}s; we

did, however, observe an effect in the skin when we experimentally controlled for environmental conditions. Moreover, respiratory viral infections result in persistent antigen presentation (Zammit et al., 2006; Jelley-Gibbs et al., 2007; Turner et al., 2007) and can contribute to the locality of memory T cells (Kim et al., 2010). Persistent antigen presentation was therefore an appealing explanation for the generation and long-term maintenance of T_{RM}s in peripheral tissues.

Here, we used inducible deletion of *B2m* to test if persistent antigen stimulation is required for maintaining skin T_{RM}s. We found that deletion of *B2m* after T_{RM} formation did not affect the number of T_{RM}s, suggesting that local cognate antigen or even low-level stimulation from cross-reactive pMHCI complexes is not required for T_{RM} maintenance. However, since our studies focused on the $CD45^+$ compartment, it is possible that low-level expression of MHCI on nonhematopoietic cells could contribute to T_{RM} maintenance. Nonetheless, our results add to previous reports (Casey et al., 2012; Mackay et al., 2012; Shin and Iwasaki, 2012; Davies et al., 2017; Slütter et al., 2017) by suggesting that T_{RM} maintenance is also apparently independent of cross-reactive pMHCI complexes.

Collectively, our findings shed light on the maintenance, generation, and activation of $CD8^+$ T_{RM}s and highlight the effects of viral MHCI inhibition on T_{RM} biology. The effects of viral MHCI inhibition on $CD8^+$ T cells can be difficult to demonstrate, as most of the identified viral MHCI inhibitors exhibit varying degrees of species specificity and efficacy across MHCI allomorphs (Cox et al., 1994; Le Gall et al., 1998; Rehm et al., 2002; Wagner et al., 2002). Remarkably, CPXV012 and CPXV203 potently act on both murine and human MHCI molecules, and the in vivo effects on $CD8^+$ T cell responses are evident. The CPXV infection model thus provides a unique opportunity to investigate the effects of viral immune evasion on antiviral $CD8^+$ T cell development and effector functions. Although we demonstrate that CPXV-mediated MHCI inhibition evades $CD8^+$ T_{RM} responses, the relevance of skin T_{RM} responses following CPXV reinfection of its natural wild rodent hosts or humans is unclear. For instance, skin T_{RM}s would only be activated if CPXV reinfection occurred at or by sites of previous infections where T_{RM}s have formed. In contrast, T_{RM}s may be relevant for natural CPXV reinfections acquired through respiratory routes, where lung T_{RM}s are more likely to reencounter viral antigens. In the case of the later, the role CPXV012 and CPXV203 would certainly be advantageous for the virus. Given the efficacy of CPXV012 and CPXV203, it is likely that CPXV-mediated MHCI inhibition also contributes to the evasion of T_{CM}s and T_{EM}s, but we did not directly test this. Nonetheless, our study demonstrates a proof of concept that viral inhibition of MHCI antigen presentation can affect memory $CD8^+$ T cell development and responses, which should be considered in regards to vaccine design against viruses that target the MHCI pathway.

Materials and methods

Mice, cell lines, and viruses

C57BL/6 mice were purchased from the National Cancer Institute. Transgenic and knockout mice were purchased from The Jackson Laboratory, with the exception of $B2m^{fl/fl}$ and IFNγ KI Thy1.1 mice. IFNγ KI Thy1.1 mice were provided by Dr. Casey Weaver (University of Alabama School of Medicine, Birmingham, AL). $B2m^{fl/fl}$ mice were generated as described by Bern et al. (2018). DC2.4 cells were cultured in RPMI supplemented with 10% FBS (Mediatech), 100 U/ml penicillin, 100 g/ml streptomycin, 1 mM sodium pyruvate, L-glutamine, and nonessential amino acids (Gibco). Madin–Darby Canine Kidney (MDCK) and Vero cells were maintained in MEM with 5% FBS, MEM vitamins (Gibco), L-glutamine, 100 U/ml penicillin, and 100 g/ml streptomycin. Human embryonic kidney cells (293T) were maintained in Opti-MEM (Life Technologies) with 10% FBS, L-glutamine, 100 U/ml penicillin, and 100 g/ml streptomycin. DC2.4 cells were a gift from Dr. Kenneth Rock (University of Massachusetts Medical School, Worchester, MA). MDCK and 293T cells were a gift from Dr. Richard Webby (St. Jude Children's Research Hospital, Memphis, TN). Vero cells were obtained from the American Type Culture Collection.

For the generation of IAV-$B8_{19–26}$ (Flu-B8), the CPXV $B8_{19–26}$ epitope was inserted into the stalk region of neuraminidase, in-frame, between nucleotides 148 and 170 using inverse PCR (Phusion-HF; Thermo Fisher) and the restriction enzyme AarI (Thermo Fisher) to ligate the mutant plasmid. Co-cultures of 293T and MDCK cells were transfected with eight bidirectional pHW2000 plasmids containing cDNA for A/Puerto Rico/08/1934 (H1N1; 1 µg per plasmid) with polyethylenimine (8 µg total). Rescue of the reverse genetic virus was performed as previously described (Williams et al., 2018).

Bacterial artificial chromosome–derived CPXV viruses were generated as previously described (Lauron et al., 2018). To determine viral titers, tissues were processed as previously described (Gainey et al., 2012). In brief, harvested tissues were placed in 1 ml MEM, homogenized using a MiniBeadbeater-8, and stored at −80°C. Samples were then serially diluted for plaque assays using Vero cells.

Mouse infection and parabiosis surgery

Mice 8–10 wk of age were sex and age matched for each experiment. i.n. and s.s. infections were performed as previously described (Gainey et al., 2012). In brief, mice were anesthetized, and 30 µl of virus inoculum diluted in PBS was administered i.n. For s.s., fur from the flank of mice was depilated using Nair. The following day, mice were anesthetized and the flanks were infected by s.s. at three adjacent sites with 10^5 PFU per site. Parabiosis surgery was performed as previously described (Peng et al., 2013; Sojka et al., 2014). Parabiosed mice were rested for 2 wk before sacrificing and harvesting tissues. Mouse studies were approved by the Animal Studies Committee at Washington University (protocol #A-3381-01) and adhered to the Institutional Animal Care and Use Committee guidelines.

Immunofluorescence

A 2 × 3 cm^2 piece of skin was harvested from infected mice and prepared as previously described (Hsu et al., 2009). Sections were blocked using 10% goat serum in PBS for 1 h before incubating with primary antibodies for 1 h. Cells were then washed with 0.5% Triton in PBS, incubated with Streptavidin-AF555

(Thermo Fisher), washed with 0.5% Triton in PBS, and mounted with DAPI (Vectashield). Stained sections were analyzed with a laser scanning confocal microscope (LSM880; Zeiss). Primary antibodies were obtained from BD PharMingen and include CD103-Biotin (M290), IA/IE-AF647 (M5/114.15.2), and CD8α-AF488 (53–6.7).

In vivo antibody, FTY720, cidofovir, and tamoxifen treatment

To induce TCR ligation in vivo, 50 µg anti-CD3e monoclonal antibody (145-2C11; Thermo Fisher) was administered into mice by i.v. injection 16 h before harvesting tissues. FTY720 (Cayman Chemical) was administered by i.p. injection (10 mg/kg) in aqueous solution. A 1% cidofovir solution (Sigma-Aldrich) was prepared in DMSO, and 16 µl per lesion was applied topically on 3 dpi and twice daily for the remaining time points indicated. To deplete $CD4^+$ T cells, 200 µg anti-CD4 (GK1.5) or isotype control (anti-rat IgG2b; Bio X Cell) was injected i.p. To deplete natural killer (NK) cells, 100 µg anti-NK1.1 (PK136) was injected i.p. weekly. For IV staining, fluorochrome-conjugated anti-CD45.2 (104; BioLegend) was administered by i.v. injection. 3 min after injection, mice were sacrificed, and tissues were harvested. Mice were treated topically with 1 mg 4-hydroxytamoxifen (Sigma-Aldrich) dissolved in ethanol and were fed a tamoxifen diet (Envigo) during the indicated times shown.

Flow cytometry, intracellular cytokine staining, antibodies, and cell sorting

Single-cell suspensions from the spleens, lymph nodes, and lungs and an ∼2 × 3 cm^2 piece of skin were prepared at the indicated days after infection as previously described (Gainey et al., 2012; Jiang et al., 2012). Skin and lung tissues were minced and incubated in with HBSS containing 1 mg/ml collagenase A (Roche) and 22.4 g/ml DNase I (Roche) at 37°C for 30 min. Samples were then filtered through a 70-µm mesh strainer before staining. For IL-10 staining, cells were incubated in RPMI containing GolgiPlug (BD Biosciences) at 37°C for 2 h before staining. Samples for flow cytometric analyses were stained on ice with Fixable Viability Dye eFlour 506 (eBioscience) before tetramer and cell surface staining. For tetramer staining, cells were incubated with tetramers for 45 min at room temperature before cell surface staining of the indicated surface markers. Tetramers were produced in the Immunomonitoring Laboratory within the Center for Human Immunology and Immunotherapy Programs (Washington University). Ex vivo restimulation and intracellular cytokine staining for IFN-γ was performed as previously described (Lauron et al., 2018). For staining of Nur77, the Foxp3/Transcription Factor Staining Buffer Set was used according to the manufacturer's protocol (eBioscience). The following antibodies were purchased from Abcam, BD Biosciences, eBioscience, BioLegend, or Thermo Fisher: CD3 (145-2C11), NK1.1 (PK136), CD19 (eBio1D3), CD64 (X54-5/7.1), CD8α (53–6.7), CD4 (RM4-5), VACV (Ab19970), CD4 (RM4-4), CD44 (IM7), CD103 (2E7), CD69 (H1.2F3), H-$2K^b$ (AF-88.5), CD11c (N418), CD45.1 (A20), CD45.2 (104), CD24 (M1/69), IA/IE (M5/114.15.2), SIRPα (P84), CD11b (M1/70), Ly6C (HK1.4), Nur77 (12.14), and IL-10 (JES5-16E3). Cell sorting was performed on a BD FACSAria Fusion sorter.

RNA isolation and RNA-seq analysis

$B8_{19–26}$-specific $CD8^+$ T cells (LIVE/$DEAD^-CD4^-CD45.2^+CD3^+CD8^+CD44^+B8_{19–26}$-$tetramer^+$) were sorted from the spleen and skin of mice coinfected on opposite flanks with WT CPXV and Δ12Δ203 at 7 dpi. Cells were pooled from five mice per experiment to reach at least 20,000 cells per sample. RNA was extracted using the Arcturus PicoPure RNA Isolation kit according to the manufacturer's protocol (Thermo Fisher). mRNA-seq libraries were created using SMARTer cDNA synthesis technology (Clontech), indexed, pooled, and sequenced at the Genome Technology Access Center (GTAC) at Washington University School of Medicine (St. Louis, MO). Sequencing was run as paired-end reads of 100 bp on the Illumina HiSeq 2500 platform. Raw reads were deposited in the National Center for Biotechnology Information Sequence Read Archive (BioProject ID: PRJNA498691; BioSample accession nos. SAMN10330286, SAMN10330287, SAMN10330288, SAMN10330289, SAMN10330290, and SAMN10330291). Basecalls and demultiplexing were performed with Illumina's bcl2fastq software and a custom python demultiplexing program with a maximum of one mismatch in the indexing read. RNA-seq reads were then aligned using STAR aligner (Dobin et al., 2013). Gene counts were derived from the number of uniquely aligned unambiguous reads by Subread: featureCount (Liao et al., 2014) and subsequently analyzed using DESeq2 (Love et al., 2014). GSEAs were performed using the GenePattern module GSEAPreranked.

In vivo cytotoxicity assay

Mice were infected by s.s. with WT CPXV. At 6 dpi, infected mice and naive controls were injected i.p. with 200 µg/mouse of α-NK1.1. At 7 dpi, DC2.4 cells were mock-infected or infected with CPXV (multiplicity of infection of 2) and incubated at 37°C for 2.5 h. Cells were then washed with PBS and costained with CellTrace Far Red dye and either 20 µM, 4 µM, or 0.8 µM CellTrace Violet dye (Thermo Fisher). Labeled cells were transferred i.v. (10^6 cells per group) into naive mice or day 7–infected mice. After 4 h, the lungs were harvested as described above and cells were examined by flow cytometry. Far Red^+ cells were gated, and the percent killing was calculated using the following formula: 100 − ([(% infected cells in infected mice/% mock-infected in infected mice)/(% infected cells in naive mice/% mock-infected in naive mice)] × 100).

Statistical analysis

The data were analyzed with an unpaired Student's *t* test or one-way ANOVA followed by Tukey's post-test comparison using Prism GraphPad software.

Online supplemental material

Fig. S1 shows that skin $CD8^+$ T cells up-regulate local IL-10 production during acute CPXV infection. Fig. S2 shows that local antigen recognition up-regulates CD69 and Nur77 expression by $CD8^+$ T cells. Fig. S3 shows that $CD8^+$ T_{RM}s develop without continuous recruitment of $CD8^+$ T cells during acute CPXV infection. Fig. S4 shows that Flu-B8 respiratory infection generates $B8_{19–26}$-specific $CD8^+$ T_{RM}s in the lungs. Fig. S5 shows that the number of $CD8^+$ T_{RM}s is reduced in B cell–deficient mice.

Acknowledgments

We thank Sathi Wijeyesinghe and Dr. David Masopust for their technical advice regarding IV staining. We also gratefully acknowledge Dr. Herbert Virgin, Dr. Brian Edelson, Dr. David Sibley, and Dr. Haina Shin for their helpful suggestions on this study. We thank the GTAC, Department of Genetics, Washington University School of Medicine for help with RNA-seq analysis.

This work was supported by the National Institutes of Health (NIH; grant U19-AI109948 and the Initiative for Maximizing Student Development grant R25GM103757), the Chancellor's Graduate Fellowship, and the American Society for Microbiology Robert D. Watkins Graduate Research Fellowship. The GTAC is partially supported by the National Cancer Institute (Cancer Center Support grant P30 CA91842 to the Siteman Cancer Center) and by the National Center for Research Resources, a component of the NIH (ICTS/CTSA grant ULTR002345), and NIH Roadmap for Medical Research. This publication is solely the responsibility of the authors and does not necessarily represent the official view of the National Center for Research Resources or NIH.

The authors declare no competing financial interests.

Author contributions: E.J. Lauron, L. Yang, I.B. Harvey, D.K. Sojka, G.D. Williams, M.A. Paley, M.D. Bern, E. Park, F. Victorino, A.C.M. Boon, and W.M. Yokoyama designed, analyzed, and performed experiments. E.J. Lauron and W.M. Yokoyama wrote the manuscript.

Submitted: 8 June 2018
Revised: 14 September 2018
Accepted: 7 November 2018

References

Alzhanova, D., D.M. Edwards, E. Hammarlund, I.G. Scholz, D. Horst, M.J. Wagner, C. Upton, E.J. Wiertz, M.K. Slifka, and K. Früh. 2009. Cowpox virus inhibits the transporter associated with antigen processing to evade T cell recognition. *Cell Host Microbe.* 6:433–445. https://doi.org/10.1016/j.chom.2009.09.013

Anderson, K.G., H. Sung, C.N. Skon, L. Lefrancois, A. Deisinger, V. Vezys, and D. Masopust. 2012. Cutting edge: intravascular staining redefines lung CD8 T cell responses. *J. Immunol.* 189:2702–2706. https://doi.org/10.4049/jimmunol.1201682

Ariotti, S., M.A. Hogenbirk, F.E. Dijkgraaf, L.L. Visser, M.E. Hoekstra, J.-Y. Song, H. Jacobs, J.B. Haanen, and T.N. Schumacher. 2014. T cell memory. Skin-resident memory CD8$^+$ T cells trigger a state of tissue-wide pathogen alert. *Science.* 346:101–105. https://doi.org/10.1126/science.1254803

Asano, M.S., and R. Ahmed. 1996. CD8 T cell memory in B cell-deficient mice. *J. Exp. Med.* 183:2165–2174. https://doi.org/10.1084/jem.183.5.2165

Basta, S., W. Chen, J.R. Bennink, and J.W. Yewdell. 2002. Inhibitory effects of cytomegalovirus proteins US2 and US11 point to contributions from direct priming and cross-priming in induction of vaccinia virus-specific CD8(+) T cells. *J. Immunol.* 168:5403–5408.

Bern, M.D., B.A. Parikh, L. Yang, D.L. Beckman, J. Poursine-Laurent, and W.M. Yokoyama. 2018. Inducible down-regulation of MHC class I results in natural killer cell tolerance. *J. Exp. Med.* https://doi.org/10.1084/jem.20181076

Beura, L.K., J.S. Mitchell, E.A. Thompson, J.M. Schenkel, J. Mohammed, S. Wijeyesinghe, R. Fonseca, B.J. Burbach, H.D. Hickman, V. Vezys, et al. 2018. Intravital mucosal imaging of CD8$^+$ resident memory T cells shows tissue-autonomous recall responses that amplify secondary memory. *Nat. Immunol.* 19:173–182. https://doi.org/10.1038/s41590-017-0029-3

Boissonnas, A., F. Licata, L. Poupel, S. Jacquelin, L. Fetler, S. Krumeich, C. Théry, S. Amigorena, and C. Combadière. 2013. CD8+ tumor-infiltrating T cells are trapped in the tumor-dendritic cell network. *Neoplasia.* (15):85–94.

Brooks, D.G., K.B. Walsh, H. Elsaesser, and M.B.A. Oldstone. 2010. IL-10 directly suppresses CD4 but not CD8 T cell effector and memory responses following acute viral infection. *Proc. Natl. Acad. Sci. USA.* 107:3018–3023. https://doi.org/10.1073/pnas.0914500107

Broz, M.L., M. Binnewies, B. Boldajipour, A.E. Nelson, J.L. Pollack, D.J. Erle, A. Barczak, M.D. Rosenblum, A. Daud, D.L. Barber, et al. 2014. Dissecting the tumor myeloid compartment reveals rare activating antigen-presenting cells critical for T cell immunity. *Cancer Cell.* 26:638–652. https://doi.org/10.1016/j.ccell.2014.09.007

Byun, M., X. Wang, M. Pak, T.H. Hansen, and W.M. Yokoyama. 2007. Cowpox virus exploits the endoplasmic reticulum retention pathway to inhibit MHC class I transport to the cell surface. *Cell Host Microbe.* 2:306–315. https://doi.org/10.1016/j.chom.2007.09.002

Byun, M., M.C. Verweij, D.J. Pickup, E.J.H.J. Wiertz, T.H. Hansen, and W.M. Yokoyama. 2009. Two mechanistically distinct immune evasion proteins of cowpox virus combine to avoid antiviral CD8 T cells. *Cell Host Microbe.* 6:422–432. https://doi.org/10.1016/j.chom.2009.09.012

Carbone, F.R. 2015. Tissue-Resident Memory T Cells and Fixed Immune Surveillance in Nonlymphoid Organs. *J. Immunol.* 195:17–22. https://doi.org/10.4049/jimmunol.1500515

Casey, K.A., K.A. Fraser, J.M. Schenkel, A. Moran, M.C. Abt, L.K. Beura, P.J. Lucas, D. Artis, E.J. Wherry, K. Hogquist, et al. 2012. Antigen independent differentiation and maintenance of effector-like resident memory T cells in tissues. *J. Immunol.* 188:4866–4875. https://doi.org/10.4049/jimmunol.1200402

Cox, J.H., R.M. Buller, J.R. Bennink, J.W. Yewdell, and G. Karupiah. 1994. Expression of adenovirus E3/19K protein does not alter mouse MHC class I-restricted responses to vaccinia virus. *Virology.* 204:558–562. https://doi.org/10.1006/viro.1994.1569

Davies, B., J.E. Prier, C.M. Jones, T. Gebhardt, F.R. Carbone, and L.K. Mackay. 2017. Cutting Edge: Tissue-Resident Memory T Cells Generated by Multiple Immunizations or Localized Deposition Provide Enhanced Immunity. *J. Immunol.* 198:2233–2237. https://doi.org/10.4049/jimmunol.1601367

Dobin, A., C.A. Davis, F. Schlesinger, J. Drenkow, C. Zaleski, S. Jha, P. Batut, M. Chaisson, and T.R. Gingeras. 2013. STAR: ultrafast universal RNA-seq aligner. *Bioinformatics.* 29:15–21. https://doi.org/10.1093/bioinformatics/bts635

Gainey, M.D., J.G. Rivenbark, H. Cho, L. Yang, and W.M. Yokoyama. 2012. Viral MHC class I inhibition evades CD8+ T-cell effector responses in vivo but not CD8+ T-cell priming. *Proc. Natl. Acad. Sci. USA.* 109:E3260–E3267. https://doi.org/10.1073/pnas.1217111109

Gebhardt, T., L.M. Wakim, L. Eidsmo, P.C. Reading, W.R. Heath, and F.R. Carbone. 2009. Memory T cells in nonlymphoid tissue that provide enhanced local immunity during infection with herpes simplex virus. *Nat. Immunol.* 10:524–530. https://doi.org/10.1038/ni.1718

Hansen, T.H., and M. Bouvier. 2009. MHC class I antigen presentation: learning from viral evasion strategies. *Nat. Rev. Immunol.* 9:503–513. https://doi.org/10.1038/nri2575

Hansen, S.G., C.J. Powers, R. Richards, A.B. Ventura, J.C. Ford, D. Siess, M.K. Axthelm, J.A. Nelson, M.A. Jarvis, L.J. Picker, and K. Früh. 2010. Evasion of CD8+ T cells is critical for superinfection by cytomegalovirus. *Science.* 328:102–106. https://doi.org/10.1126/science.1185350

Hsu, K.M., J.R. Pratt, W.J. Akers, S.I. Achilefu, and W.M. Yokoyama. 2009. Murine cytomegalovirus displays selective infection of cells within hours after systemic administration. *J. Gen. Virol.* 90:33–43. https://doi.org/10.1099/vir.0.006668-0

Iborra, S., M. Martínez-López, S.C. Khouili, M. Enamorado, F.J. Cueto, R. Conde-Garrosa, C. Del Fresno, and D. Sancho. 2016. Optimal Generation of Tissue-Resident but Not Circulating Memory T Cells during Viral Infection Requires Crosspriming by DNGR-1$^+$ Dendritic Cells. *Immunity.* 45:847–860. https://doi.org/10.1016/j.immuni.2016.08.019

Jelley-Gibbs, D.M., J.P. Dibble, D.M. Brown, T.M. Strutt, K.K. McKinstry, and S.L. Swain. 2007. Persistent depots of influenza antigen fail to induce a cytotoxic CD8 T cell response. *J. Immunol.* 178:7563–7570.

Jiang, X., R.A. Clark, L. Liu, A.J. Wagers, R.C. Fuhlbrigge, and T.S. Kupper. 2012. Skin infection generates non-migratory memory CD8+ T(RM) cells providing global skin immunity. *Nature.* 483:227–231. https://doi.org/10.1038/nature10851

Khan, T.N., J.L. Mooster, A.M. Kilgore, J.F. Osborn, and J.C. Nolz. 2016. Local antigen in nonlymphoid tissue promotes resident memory CD8+ T cell formation during viral infection. *J. Exp. Med.* 213:951–966. https://doi.org/10.1084/jem.20151855

Kim, T.S., M.M. Hufford, J. Sun, Y.-X. Fu, and T.J. Braciale. 2010. Antigen persistence and the control of local T cell memory by migrant respiratory dendritic cells after acute virus infection. *J. Exp. Med.* 207:1161–1172. https://doi.org/10.1084/jem.20092017

Laidlaw, B.J., N. Zhang, H.D. Marshall, M.M. Staron, T. Guan, Y. Hu, L.S. Cauley, J. Craft, and S.M. Kaech. 2014. CD4+ T cell help guides formation of CD103+ lung-resident memory CD8+ T cells during influenza viral infection. *Immunity.* 41:633–645. https://doi.org/10.1016/j.immuni.2014.09.007

Lauron, E.J., L. Yang, J.I. Elliott, M.D. Gainey, D.H. Fremont, and W.M. Yokoyama. 2018. Cross-priming induces immunodomination in the presence of viral MHC class I inhibition. *PLoS Pathog.* 14:e1006883. https://doi.org/10.1371/journal.ppat.1006883

Lee, Y.-T., J.E. Suarez-Ramirez, T. Wu, J.M. Redman, K. Bouchard, G.A. Hadley, and L.S. Cauley. 2011. Environmental and antigen receptor-derived signals support sustained surveillance of the lungs by pathogen-specific cytotoxic T lymphocytes. *J. Virol.* 85:4085–4094. https://doi.org/10.1128/JVI.02493-10

Le Gall, S., L. Erdtmann, S. Benichou, C. Berlioz-Torrent, L. Liu, R. Benarous, J.M. Heard, and O. Schwartz. 1998. Nef interacts with the mu subunit of clathrin adaptor complexes and reveals a cryptic sorting signal in MHC I molecules. *Immunity.* 8:483–495. https://doi.org/10.1016/S1074-7613(00)80553-1

Liao, Y., G.K. Smyth, and W. Shi. 2014. featureCounts: an efficient general purpose program for assigning sequence reads to genomic features. *Bioinformatics.* 30:923–930. https://doi.org/10.1093/bioinformatics/btt656

Love, M.I., W. Huber, and S. Anders. 2014. Moderated estimation of fold change and dispersion for RNA-seq data with DESeq2. *Genome Biol.* 15:550. https://doi.org/10.1186/s13059-014-0550-8

Lu, X., A.K. Pinto, A.M. Kelly, K.S. Cho, and A.B. Hill. 2006. Murine cytomegalovirus interference with antigen presentation contributes to the inability of CD8 T cells to control virus in the salivary gland. *J. Virol.* 80:4200–4202. https://doi.org/10.1128/JVI.80.8.4200-4202.2006

Mackay, L.K., A.T. Stock, J.Z. Ma, C.M. Jones, S.J. Kent, S.N. Mueller, W.R. Heath, F.R. Carbone, and T. Gebhardt. 2012. Long-lived epithelial immunity by tissue-resident memory T (TRM) cells in the absence of persisting local antigen presentation. *Proc. Natl. Acad. Sci. USA.* 109:7037–7042. https://doi.org/10.1073/pnas.1202288109

McMaster, S.R., A.N. Wein, P.R. Dunbar, S.L. Hayward, E.K. Cartwright, T.L. Denning, and J.E. Kohlmeier. 2018. Pulmonary antigen encounter regulates the establishment of tissue-resident CD8 memory T cells in the lung airways and parenchyma. *Mucosal Immunol.* 11:1071–1078. https://doi.org/10.1038/s41385-018-0003-x

Moran, A.E., K.L. Holzapfel, Y. Xing, N.R. Cunningham, J.S. Maltzman, J. Punt, and K.A. Hogquist. 2011. T cell receptor signal strength in Treg and iNKT cell development demonstrated by a novel fluorescent reporter mouse. *J. Exp. Med.* 208:1279–1289. https://doi.org/10.1084/jem.20110308

Muschaweckh, A., V.R. Buchholz, A. Fellenzer, C. Hessel, P.-A. König, S. Tao, R. Tao, M. Heikenwälder, D.H. Busch, T. Korn, et al. 2016. Antigen-dependent competition shapes the local repertoire of tissue-resident memory CD8+ T cells. *J. Exp. Med.* 213:3075–3086. https://doi.org/10.1084/jem.20160888

Peng, H., X. Jiang, Y. Chen, D.K. Sojka, H. Wei, X. Gao, R. Sun, W.M. Yokoyama, and Z. Tian. 2013. Liver-resident NK cells confer adaptive immunity in skin-contact inflammation. *J. Clin. Invest.* 123:1444–1456. https://doi.org/10.1172/JCI66381

Pizzolla, A., T.H.O. Nguyen, J.M. Smith, A.G. Brooks, K. Kedzieska, W.R. Heath, P.C. Reading, and L.M. Wakim. 2017. Resident memory CD8$^+$ T cells in the upper respiratory tract prevent pulmonary influenza virus infection. *Sci. Immunol.* 2:eaam6970. https://doi.org/10.1126/sciimmunol.aam6970

Rehm, A., A. Engelsberg, D. Tortorella, I.J. Körner, I. Lehmann, H.L. Ploegh, and U.E. Höpken. 2002. Human cytomegalovirus gene products US2 and US11 differ in their ability to attack major histocompatibility class I heavy chains in dendritic cells. *J. Virol.* 76:5043–5050. https://doi.org/10.1128/JVI.76.10.5043-5050.2002

Schenkel, J.M., K.A. Fraser, L.K. Beura, K.E. Pauken, V. Vezys, and D. Masopust. 2014. T cell memory. Resident memory CD8 T cells trigger protective innate and adaptive immune responses. *Science.* 346:98–101. https://doi.org/10.1126/science.1254536

Schmitz, J.E., M.J. Kuroda, S. Santra, V.G. Sasseville, M.A. Simon, M.A. Lifton, P. Racz, K. Tenner-Racz, M. Dalesandro, B.J. Scallon, et al. 1999. Control of viremia in simian immunodeficiency virus infection by CD8+ lymphocytes. *Science.* 283:857–860. https://doi.org/10.1126/science.283.5403.857

Shen, H., J.K. Whitmire, X. Fan, D.J. Shedlock, S.M. Kaech, and R. Ahmed. 2003. A specific role for B cells in the generation of CD8 T cell memory by recombinant Listeria monocytogenes. *J. Immunol.* 170:1443–1451.

Shen, X., S.B.J. Wong, C.B. Buck, J. Zhang, and R.F. Siliciano. 2002. Direct priming and cross-priming contribute differentially to the induction of CD8+ CTL following exposure to vaccinia virus via different routes. *J. Immunol.* 169:4222–4229.

Shin, H., and A. Iwasaki. 2012. A vaccine strategy that protects against genital herpes by establishing local memory T cells. *Nature.* 491:463–467. https://doi.org/10.1038/nature11522

Shin, H., Y. Kumamoto, S. Gopinath, and A. Iwasaki. 2016. CD301b+ dendritic cells stimulate tissue-resident memory CD8+ T cells to protect against genital HSV-2. *Nat. Commun.* 7:13346. https://doi.org/10.1038/ncomms13346

Shoukry, N.H., A. Grakoui, M. Houghton, D.Y. Chien, J. Ghrayeb, K.A. Reimann, and C.M. Walker. 2003. Memory CD8+ T cells are required for protection from persistent hepatitis C virus infection. *J. Exp. Med.* 197:1645–1655. https://doi.org/10.1084/jem.20030239

Simon, C.O., R. Holtappels, H.-M. Tervo, V. Böhm, T. Däubner, S.A. Oehrlein-Karpi, B. Kühnapfel, A. Renzaho, D. Strand, J. Podlech, et al. 2006. CD8 T cells control cytomegalovirus latency by epitope-specific sensing of transcriptional reactivation. *J. Virol.* 80:10436–10456. https://doi.org/10.1128/JVI.01248-06

Slütter, B., N. Van Braeckel-Budimir, G. Abboud, S.M. Varga, S. Salek-Ardakani, and J.T. Harty. 2017. Dynamics of influenza-induced lung-resident memory T cells underlie waning heterosubtypic immunity. *Sci. Immunol.* 2:eaag2031. https://doi.org/10.1126/sciimmunol.aag2031

Sojka, D.K., B. Plougastel-Douglas, L. Yang, M.A. Pak-Wittel, M.N. Artyomov, Y. Ivanova, C. Zhong, J.M. Chase, P.B. Rothman, J. Yu, et al. 2014. Tissue-resident natural killer (NK) cells are cell lineages distinct from thymic and conventional splenic NK cells. *eLife.* 3:e01659. https://doi.org/10.7554/eLife.01659

Takamura, S., H. Yagi, Y. Hakata, C. Motozono, S.R. McMaster, T. Masumoto, M. Fujisawa, T. Chikaishi, J. Komeda, J. Itoh, et al. 2016. Specific niches for lung-resident memory CD8+ T cells at the site of tissue regeneration enable CD69-independent maintenance. *J. Exp. Med.* 213:3057–3073. https://doi.org/10.1084/jem.20160938

Teijaro, J.R., D. Turner, Q. Pham, E.J. Wherry, L. Lefrançois, and D.L. Farber. 2011. Cutting edge: Tissue-retentive lung memory CD4 T cells mediate optimal protection to respiratory virus infection. *J. Immunol.* 187:5510–5514. https://doi.org/10.4049/jimmunol.1102243

Thom, J.T., T.C. Weber, S.M. Walton, N. Torti, and A. Oxenius. 2015. The Salivary Gland Acts as a Sink for Tissue-Resident Memory CD8(+) T Cells, Facilitating Protection from Local Cytomegalovirus Infection. *Cell Reports.* 13:1125–1136. https://doi.org/10.1016/j.celrep.2015.09.082

Turner, D.L., L.S. Cauley, K.M. Khanna, and L. Lefrançois. 2007. Persistent antigen presentation after acute vesicular stomatitis virus infection. *J. Virol.* 81:2039–2046. https://doi.org/10.1128/JVI.02167-06

Wagner, M., A. Gutermann, J. Podlech, M.J. Reddehase, and U.H. Koszinowski. 2002. Major histocompatibility complex class I allele-specific cooperative and competitive interactions between immune evasion proteins of cytomegalovirus. *J. Exp. Med.* 196:805–816. https://doi.org/10.1084/jem.20020811

Wakim, L.M., A. Woodward-Davis, and M.J. Bevan. 2010. Memory T cells persisting within the brain after local infection show functional adaptations to their tissue of residence. *Proc. Natl. Acad. Sci. USA.* 107:17872–17879. https://doi.org/10.1073/pnas.1010201107

Williams, G.D., D. Townsend, K.M. Wylie, P.J. Kim, G.K. Amarasinghe, S.B. Kutluay, and A.C.M. Boon. 2018. Nucleotide resolution mapping of influenza A virus nucleoprotein-RNA interactions reveals RNA features required for replication. *Nat. Commun.* 9:465. https://doi.org/10.1038/s41467-018-02886-w

Wu, T., Y. Hu, Y.-T. Lee, K.R. Bouchard, A. Benechet, K. Khanna, and L.S. Cauley. 2014. Lung-resident memory CD8 T cells (TRM) are indispensable for optimal cross-protection against pulmonary virus infection. *J. Leukoc. Biol.* 95:215–224. https://doi.org/10.1189/jlb.0313180

Zaid, A., L.K. Mackay, A. Rahimpour, A. Braun, M. Veldhoen, F.R. Carbone, J.H. Manton, W.R. Heath, and S.N. Mueller. 2014. Persistence of skin-resident memory T cells within an epidermal niche. *Proc. Natl. Acad. Sci. USA.* 111:5307–5312. https://doi.org/10.1073/pnas.1322292111

Zammit, D.J., D.L. Turner, K.D. Klonowski, L. Lefrançois, and L.S. Cauley. 2006. Residual antigen presentation after influenza virus infection affects CD8 T cell activation and migration. *Immunity.* 24:439–449. https://doi.org/10.1016/j.immuni.2006.01.015

Zens, K.D., J.K. Chen, and D.L. Farber. 2016. Vaccine-generated lung tissue-resident memory T cells provide heterosubtypic protection to influenza infection. *JCI Insight.* 1:e85832. https://doi.org/10.1172/jci.insight.85832